Immunity

Integrating population and single-cell variations in vaccine responses identifies a naturally adjuvanted human immune setpoint

Graphical abstract

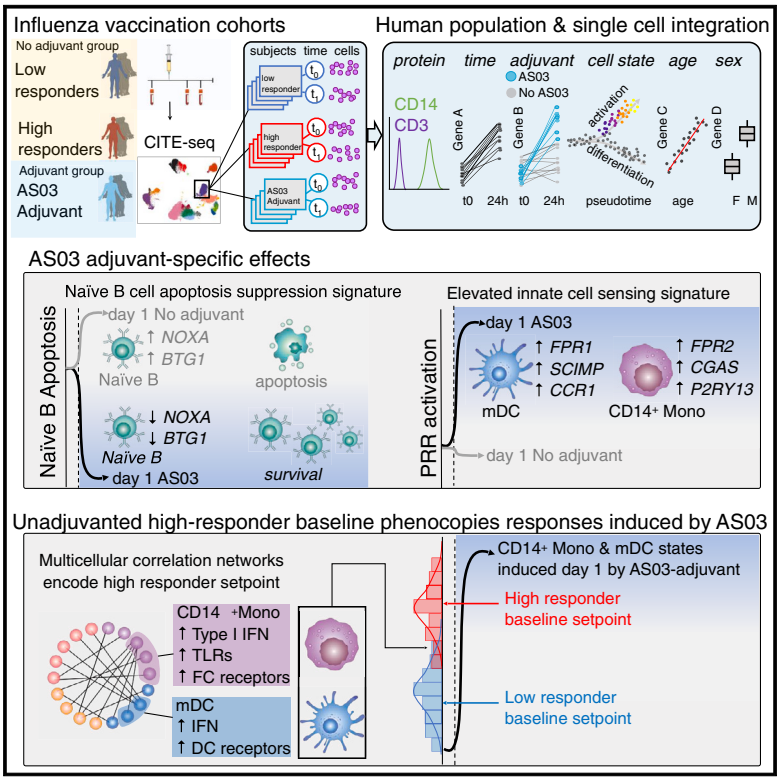

Highlights

- A framework for integrating human population and single-cell immune response variations
- AS03 induces unique B cell survival and innate-sensing and activation states
- Baseline immune setpoints are encoded as correlated networks of cell states
- A high-responder baseline setpoint phenocopies cell states induced by AS03

Authors

Matthew P. Mulè, Andrew J. Martins, Foo Cheung, ..., Jinguo Chen, Pamela L. Schwartzberg, John S. Tsang

Correspondence

john.tsang@yale.edu

In brief

Mulè et al. provide a framework for integrating human population and single-cell variations to study vaccine responses with and without the adjuvant AS03. They uncover AS03-specific B cell survival and innate-sensing signatures 1 day after vaccination. Furthermore, some AS03-induced response cell states are already present at baseline in "naturally adjuvanted" individuals who respond more robustly serologically to the unadjuvanted vaccine.

Mulè et al., 2024, Immunity *57*, 1–17
May 14, 2024 © 2024 Published by Elsevier Inc.
https://doi.org/10.1016/j.immuni.2024.04.009

CellPress

Please cite this article in press as: Mulè et al., Integrating population and single-cell variations in vaccine responses identifies a naturally adjuvanted human immune setpoint, Immunity (2024), https://doi.org/10.1016/j.immuni.2024.04.009

Immunity

CellPress

Resource

Integrating population and single-cell variations in vaccine responses identifies a naturally adjuvanted human immune setpoint

Matthew P. Mulè,[1,2] Andrew J. Martins,[1,6] Foo Cheung,[3] Rohit Farmer,[3] Brian A. Sellers,[3] Juan A. Quiel,[3] Arjun Jain,[1] Yuri Kotliarov,[3] Neha Bansal,[1] Jinguo Chen,[3] Pamela L. Schwartzberg,[4,5] and John S. Tsang[1,3,7,8,*]

[1]Multiscale Systems Biology Section, Laboratory of Immune System Biology, NIAID, NIH, Bethesda, MD, USA
[2]NIH-Oxford-Cambridge Scholars Program, Department of Medicine, University of Cambridge, Cambridge, UK
[3]NIH Center for Human Immunology, NIAID, NIH, Bethesda, MD, USA
[4]National Human Genome Research Institute, National Institutes of Health, Bethesda, MD, USA
[5]Cell Signaling and Immunity Section, NIAID, NIH, Bethesda, MD, USA
[6]Present address: Center for Systems and Engineering Immunology, Department of Immunobiology, Yale University School of Medicine, New Haven, CT, USA
[7]Present address: Center for Systems and Engineering Immunology, Department of Immunobiology, and Department of Biomedical Engineering, Yale University, New Haven, CT, USA
[8]Lead contact
*Correspondence: john.tsang@yale.edu
https://doi.org/10.1016/j.immuni.2024.04.009

SUMMARY

Multimodal single-cell profiling methods can capture immune cell variations unfolding over time at the molecular, cellular, and population levels. Transforming these data into biological insights remains challenging. Here, we introduce a framework to integrate variations at the human population and single-cell levels in vaccination responses. Comparing responses following AS03-adjuvanted versus unadjuvanted influenza vaccines with CITE-seq revealed AS03-specific early (day 1) response phenotypes, including a B cell signature of elevated germinal center competition. A correlated network of cell-type-specific transcriptional states defined the baseline immune status associated with high antibody responders to the unadjuvanted vaccine. Certain innate subsets in the network appeared "naturally adjuvanted," with transcriptional states resembling those induced uniquely by AS03-adjuvanted vaccination. Consistently, CD14^{+} monocytes from high responders at baseline had elevated phospho-signaling responses to lipopolysaccharide stimulation. Our findings link baseline immune setpoints to early vaccine responses, with positive implications for adjuvant development and immune response engineering.

INTRODUCTION

Human immune systems exhibit substantial person-to-person variation.[1–4] Population variations in immune response outcomes to the same perturbation, such as antibody responses to vaccination, can be linked to cellular and molecular immune system components using top-down systems biology approaches.[4,5] Such unbiased immune profiling has identified cellular and molecular signatures correlated with response outcomes such as antigen-specific antibody or T cell levels,[6–14] and has uncovered contributions from individual intrinsic factors, such as genetics,[15] age,[16,17] and sex.[18] Accumulating evidence from these studies supports the hypothesis that immune system status prior to a perturbation, beyond states linked to those intrinsic variables, can predict and potentially determine both response quality and quantity.[6,16,19–23] For example, we previously identified transcriptional signatures reflecting an immune system "setpoint" predictive of higher antibody response following vaccination in healthy individuals[22]; the same signature evaluated in lupus patients during disease remission was also linked to later increases plasma cell-related transcriptomic activity during disease flares. More recently, transcriptome-based setpoint prognostic signatures have been defined in healthy children prior to type 1 diabetes onset,[24] in cancer patients at risk immunotherapy-induced autoimmunity[25,26] and in healthy recovered males following COVID-19 infection, which shaped baseline immune status to impact influenza vaccination responses.[27]

Although biomarker signatures identified thus far are informative, technological limitations hinder a holistic view of immune cell processes underlying the immune setpoints that predict and potentially determine optimal responses.[28,29] Bulk blood transcriptomic profiles are confounded by substantial inter-individual variations in circulating immune cell subset frequency,[6,30,31] while flow cytometry alone cannot comprehensively assess internal cell states captured by transcriptomics. Single-cell transcriptomics can better resolve cell states but does not fully utilize existing knowledge of surface protein

Please cite this article in press as: Mulè et al., Integrating population and single-cell variations in vaccine responses identifies a naturally adjuvanted human immune setpoint, Immunity (2024), https://doi.org/10.1016/j.immuni.2024.04.009

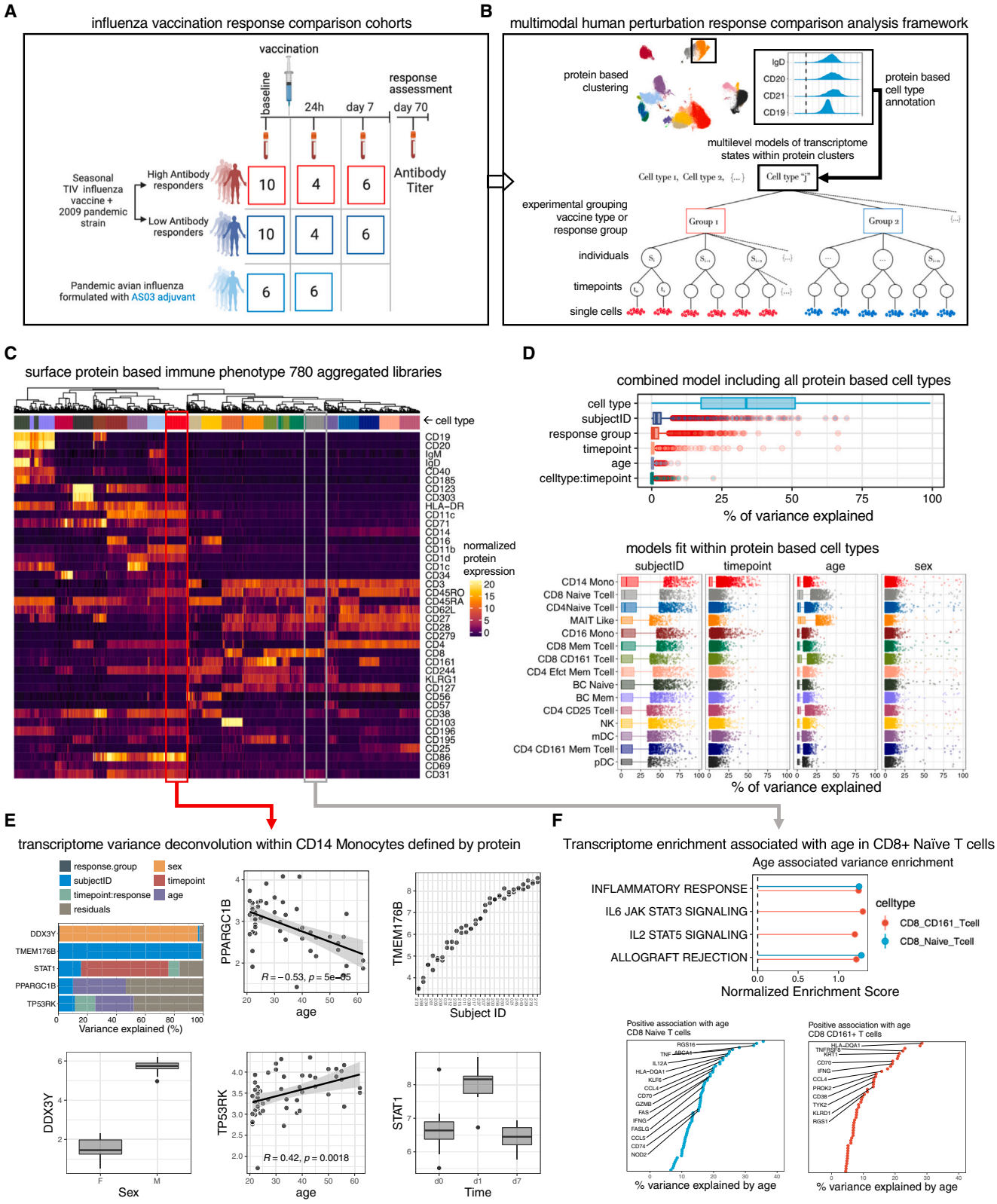

Figure 1. Multimodal single-cell portraits of human vaccination responses

(A) Human vaccination response study outline; CITE-seq data were generated from *n* = 52 PBMC samples from *n* = 26 subjects including 2 response groups for those who received the unadjuvanted vaccine and 2 vaccine formulations. Numbers in boxes indicate the number of samples run with CITE-seq. 10 high and 10

(legend continued on next page)

Please cite this article in press as: Mulè et al., Integrating population and single-cell variations in vaccine responses identifies a naturally adjuvanted human immune setpoint, Immunity (2024), https://doi.org/10.1016/j.immuni.2024.04.009

markers defining immune cell types and subsets.[6,30–32] Multimodal single-cell transcriptome and protein profiling methods such as cellular indexing of transcriptomes and epitopes sequencing (CITE-seq)[33] are promising for unifying these modalities. However, integrative analysis of timed perturbation responses, including decomposition of biological variations spanning multiple scales from individual human subjects to cell types to single cells, remains a challenge. Biologically, we also still lack understanding of how baseline immune states shape response quality and quantity to perturbations such as vaccination and infection in humans.[21,34] A better understanding of these processes can inform vaccine and adjuvant development and immune response engineering in health and disease.

In this work, we developed a multilevel modeling framework to integrate human population, temporal, and single-cell variations. We applied this framework to multimodal single-cell data to quantitatively attribute cell-type-specific transcriptomic variations to age, sex, subject, time, and an adjuvant. Our data include CITE-seq[33] profiling of PBMCs from 26 healthy subjects before and after vaccination with two different influenza vaccines: an H5N1 vaccine formulated with the adjuvant AS03 (unpublished data) and the 2009 pandemic (p2009) + seasonal trivalent inactivated influenza (TIV) H1N1 influenza vaccine without adjuvant. Application of our framework to these and additional validation data revealed previously unknown, cell-type-specific phenotypes specifically induced early by AS03.[35] Comparative analysis of AS03-specific signatures and the baseline setpoint predictors of high antibody responses to the unadjuvanted vaccine revealed that healthy, high responders have naturally adjuvanted baseline states resembling those specifically induced by day 1 after AS03 vaccination. These observations were further supported by *in vitro* cell stimulation experiments. Our integrative approach paves the way for multiscale analysis of timed perturbation studies using multimodal single-cell data in humans. Furthermore, our findings suggest cell-type-specific targets for immune response engineering and vaccine development.

RESULTS

CITE-seq data deconvolve known immune response signatures

To generate a multimodal single-cell dataset that captured biological variations spanning molecular and cellular states, vaccine formulations, inter- and intra-subject differences, and response kinetics, we assessed 52 PBMC samples from 26 donors pre and post vaccination using CITE-seq (Figure 1A). Subjects received either the 2009 seasonal and pandemic H1N1 vaccine combination without adjuvant or an H5N1 avian influenza vaccine formulated with an oil-in-emulsion adjuvant AS03.[6,36] We profiled both the baseline (before vaccination) and day 1 (post vaccination) time points for the AS03 group since AS03 is known to elicit a strong early response.[37,38] For the unadjuvanted group, we selected twenty subjects with high (n = 10) and low (n = 10) antibody responses from our cohort of 63 individuals previously stratified into high, mid, and low responders based on antibody titer fold-change adjusted for age, sex, ethnicity, and pre-existing immunity.[6,22] We profiled all 20 individuals at baseline and a subset on days 1 or 7 post vaccination to assess early innate and adaptive cellular responses (Figure 1A). We removed sources of technical noise in CITE-seq surface protein expression data with our normalization method called dsb,[39] then assessed the robustness of CITE-seq to recover and unify known cell surface and transcriptome phenotypes. For example, activated B cells and plasmablasts could be distinguished based on expression of CITE-seq surface protein markers CD19, CD71, CD20, and CD38. We further confirmed that gated subsets from CITE-seq exhibited transcriptional signatures[40] previously derived from the same cell subsets after fluorescence-activated cell sorting (FACS) (Figures S1A and S1B).

Cell type, individual, age, sex, and vaccination contribute to cell-type-specific transcriptomic variation

Cells clustered using 82 surface proteins were enriched for known immune phenotypes (Figures S1C and S1D). Cells from each subject at different time points were represented in a majority of clusters (Figures S1E and S1F). A minority of clusters, including NKT and CD57$^+$ CD4 T cells, were dominated by cells from both time points from two to three individuals, indicative of temporally stable phenotypes with relatively low within-individual and high between-individual variations[6] (Figure S1F).

Instead of analyzing one variable at a time, we next deconstructed the transcriptional variation of each gene into that attributable to cell types, individuals, intrinsic factors (age, sex), and vaccination responses (Figure 1B) using multivariate mixed effects models. For each gene, these models quantify

low responders from the 2009 TIV + pandemic H1N1 influenza vaccination without adjuvant were profiled. A subset of 8 and 12 subjects, split evenly between high and low responders, were also profiled with CITE-seq on days 1 and 7, respectively. In addition, 6 subjects vaccinated with a pandemic H5N1 influenza vaccine formulated with the adjuvant AS03 were profiled at baseline and day 1 post vaccination.

(B) The hierarchical structure of the data for a single cluster of cells is shown to motivate the multilevel mixed effects modeling approach for integration of human population and single-cell variations. Cell clusters (of "cell type") are defined based on surface protein expression (select proteins from the naive B cell cluster are shown). Clusters are represented by cells from PBMC samples indexed by individual, time point, and response (high and low responders) and vaccination (unadjuvanted vs. adjuvanted) groups.

(C) For each of the 780 pseudobulk samples (columns) aggregated by surface protein-based cell type, individual, and time point, the median dsb normalized protein expression is shown; color code for the cell types is the same as that used in (D).

(D) Top: the fraction of variance explained based on our multivariate mixed effects model; bottom: as in the top panel, but with models fit within each cell type, i.e., within each colored columns of (C).

(E) Fraction of variance explained for five example genes from the multivariate mixed effects model fit within CD14$^+$ monocytes; also shown are the expression of select genes (y axis) vs. the experimental factor (x axis) that explained the greatest variance for these five genes. Boxplot notches indicate the median, 25th and 75th percentiles. Shading represents the 95% confidence interval of the fitted line.

(F) Top: enrichment of pathways in the MSigDB Hallmark collection of gene sets based on genes ranked by their variance explained by age; subset of genes with positive association with age in CD8$^+$ naive and CD161$^+$ T cell clusters; bottom: select genes positively associated with age within the two cell types.

See also Figure S1.

Please cite this article in press as: Mulè et al., Integrating population and single-cell variations in vaccine responses identifies a naturally adjuvanted human immune setpoint, Immunity (2024), https://doi.org/10.1016/j.immuni.2024.04.009

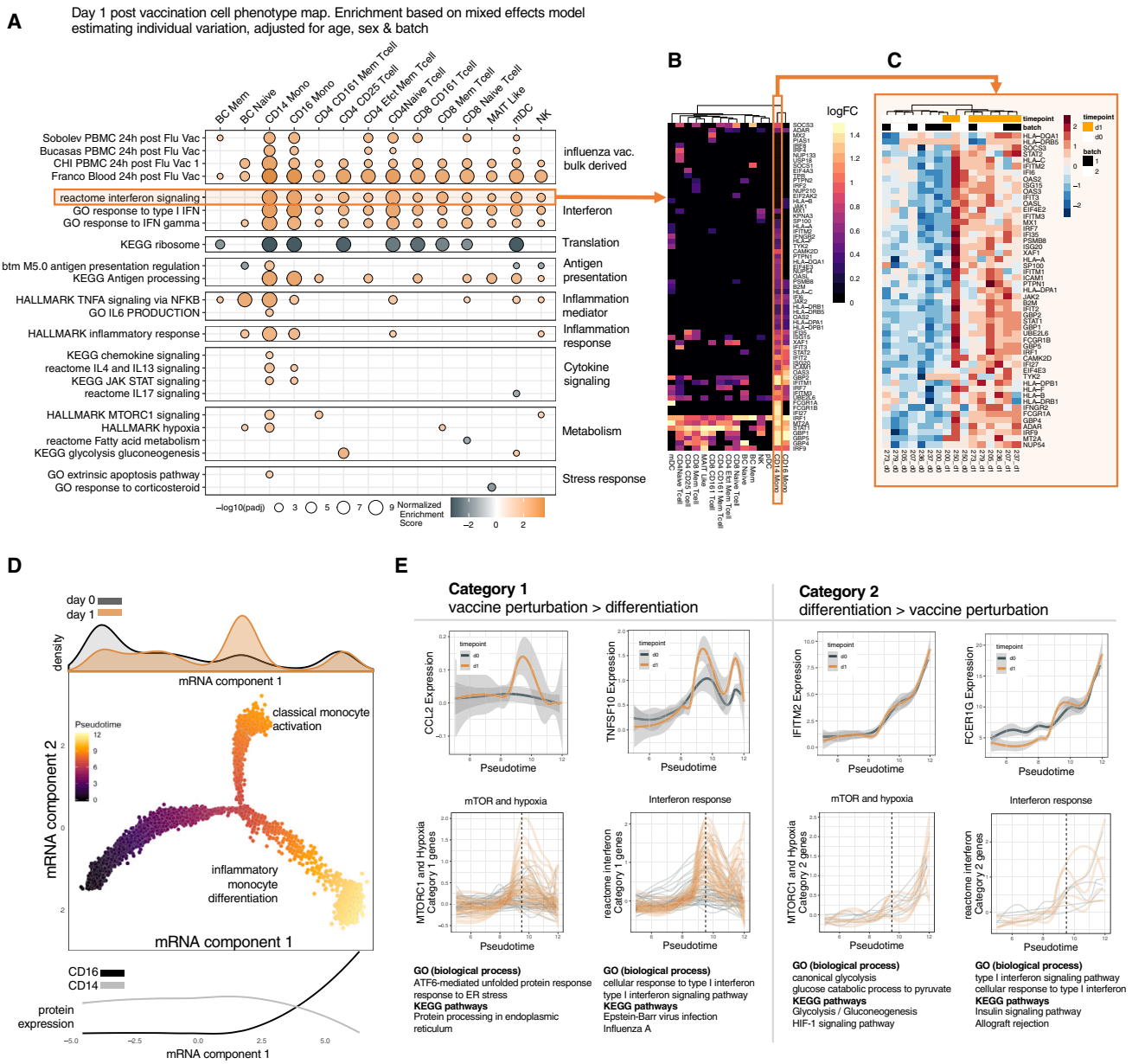

Figure 2. Multilevel modeling reveals that unadjuvanted influenza vaccination induces both cell-type-specific and -independent transcriptomic signatures

(A) Day 1 post-vaccination transcriptional response within cell types defined by surface protein expression. Gene set enrichment (orange, positive enrichment/upregulation; black, negative enrichment/downregulation) based on genes ranked by their day 1 vs. day 0 effect size inferred using pseudobulk weighted linear mixed effects models. Enriched pathways shown have adjusted p values < 0.05. The broad functional category of each curated module/pathway is labeled on the right margin; see also Table S1.

(B) Shared and cell-type-specific ISGs shown as combined leading-edge genes (rows) from the Reactome interferon signaling module. The day 1 log fold-change of a subset of these genes with day 1 mixed model p values < 0.05 and fold-change > 0.25 is shown across all cell types included in the model; see also the core interferon signature in Figures S2F and S2G.

(C) Log counts per million of aggregated data for each subject-time point combination (columns) within CD14$^+$ monocytes. Leading-edge genes are shown from the "interferon signaling" module enriched in CD14$^+$ monocytes on day 1 post vaccination, revealing coordinated upregulation of interferon signaling genes across individuals. Genes (rows) and samples (columns) were hierarchically clustered.

(D) Cells from baseline (day 0) and day 1 post vaccination were fed into the DDR-tree algorithm. Components 1 and 2 as shown are latent space embeddings based on mRNA only for single monocytes as determined by the DDR-tree algorithm. Each point is a single cell colored by pseudotime as calculated by monocle. The distribution of cells from day 1 vs. from baseline (day 0) along latent component 1 is shown in the top histogram. Three branches are evident in this 2D embedding space: the left, middle, and right branches are enriched for resting classical (CD14$^+$ CD16$^-$) monocytes, activated classical monocytes from post vaccination, and non-classical (CD14$^-$ CD16$^+$) monocytes, respectively. Cells in the rightmost branch progressively downregulate CD14 and upregulate CD16

(legend continued on next page)

Please cite this article in press as: Mulè et al., Integrating population and single-cell variations in vaccine responses identifies a naturally adjuvanted human immune setpoint, Immunity (2024), https://doi.org/10.1016/j.immuni.2024.04.009

contributions of biological factors (such as cell type or sex) toward observed expression variation, including adjusting for dependency among repeated measures from the same individuals (see STAR Methods). Models were first fit to each transcript across 780 transcriptome "pseudobulk" libraries indexed by cell type, individual, and time point (Figure 1C, columns). Cell type alone explained more than 30% of variation across the transcriptome (range 0%–100%; Figure 1D, top) in these models, consistent with observed cell-type-specific transcriptional states.[41,42] To assess contribution to transcriptional differences within but independent of those across cell types, we next fit models within cell subsets defined by surface protein expression (Figure 1D, bottom). This analysis identified factors contributing to differences within CD14$^+$ classical monocytes; five example genes are shown in Figure 1E. For example, as expected, sex almost completely explained expression variation of a Y-linked gene (DDX3Y). A transcription factor genetically linked to rheumatological pathology[43] (PPARGC1B) and an apoptosis regulator (TP53RK) were negatively and positively associated with age, respectively. We also identified between-subject variations for many genes (Figure 1D, see "SubjectID"); for example, differences among individuals accounted for nearly 100% of expression variation in TMEM176B, an inflammasome signaling regulator,[44] suggesting inflammasome function could have substantial individuality in the human population (Figure 1E). Temporal variation (i.e., differences relative to baseline following vaccination) accounted for more than 50% of the expression differences in STAT1; application of a methodologically different differential expression statistical model confirmed vaccination-induced expression of this gene within monocytes (see below). Age contributions varied across cell subsets and were particularly significant for CD8$^+$ naive and CD8$^+$ CD161$^+$ T cells; inflammatory processes were specifically enriched among genes positively correlated with age (Figure 1F), consistent with age-associated sterile inflammation.[45] Our approach provides a global view of the extent by which different biological factors contribute to gene expression variation. Variance decomposition of all genes across and within each cell type is provided in Tables S2 and S3, respectively.

CITE-seq reveals cell-type-specific early response to unadjuvanted influenza vaccination

We next deconvolved, using CITE-seq data, known signatures of vaccination response previously derived from bulk (whole blood or PBMC) measurements to identify cell-type-specific responses elicited by unadjuvanted influenza vaccination on days 1 and 7. We utilized similar mixed effects models described above to account for subject, age, sex, and technical factors (see STAR Methods). Gene set enrichment analysis revealed day 7 naive B cell and CD4$^+$ memory T cell activation and metabolic processes; though some of these effects were not significant after false discovery rate (FDR) correction and were generally weaker than early response effects described below (Figures S2A and S2B). Changes in circulating plasmablast frequencies are thought to drive whole blood transcriptome signatures measured on days 7–12 post vaccination predictive of antibody response to multiple vaccines.[6–8,46] Indeed, via CITE-seq, plasmablasts (CD38^{high} CD20$^-$ B cells) had the highest average day 7 expression of genes we compiled based on previous day 7 bulk transcriptome signatures predictive of antibody responses (Figure S2C). B cell maturation antigen (BCMA) receptor (TNFRSF17) had the highest day 7-fold-change in bulk microarray and pseudobulk CITE-seq data (Figure S2D). Deconvolution of CITE-seq sequencing reads to each cell type revealed that almost all TNFRSF17 counts were derived from CD38^{high} CD20$^-$ plasmablasts on day 7, and not from naive or memory B cells (Figure S2E).

Unadjuvanted influenza vaccination response studies consistently report interferon-stimulated gene (ISG) expression 1–3 days post vaccination in bulk blood transcriptomic data. Elevated expression of ISG and antigen presentation genes on day 1 was found to correlate with elevated antibody response,[11] although the cellular origins of such signatures were not fully resolved. Early reports profiling sorted cell subsets suggested ISG expression originated primarily from DCs on day 3[47] or monocyte/granulocytes on day 1.[13] Here, unbiased CITE-seq assessment using curated gene sets, including signatures from bulk transcriptomic studies (Table S1), identified three broad patterns of responses 24 h following vaccination. The first pattern included genes shared across cell types enriched for type I and type II interferon (IFN) signaling pathways (Figure 2A). 46 "core genes" collectively induced in at least 5 cell types (Figure S2F), included transcription factors IRF1 (notably, induced across 15 cell types), STAT1, IRF7, IRF9, pattern recognition receptor (PRR) genes IFITM1 and IFITM3, inhibitors of vial transcription GBP1[48] and ISG15,[49] and antigen presentation genes TAP1 and PSMB9 (Figure S2F). The second pattern encompassed responses unique to classical (CD14$^+$ CD16$^-$) and non-classical (CD14$^-$ CD16$^+$) monocytes, including adhesion molecule ICAM1 and JAK2, antigen presentation and human leukocyte antigen (HLA) genes, and inhibitors of viral replication OAS3[50] and ISG20[51] (Figure S2G). The third pattern reflected classical monocyte-specific responses, particularly inflammatory processes induced by vaccination (Figure S2G). The "Reactome IFN signaling" genes (Figure 2A) captured all three response patterns, with 10–15 ISGs shared across multiple cell types, including those shared by classical and non-classical monocytes, and a set of classical monocyte-specific genes

protein levels along latent component 1; curves shown in the bottom were spline fits to normalized levels for CD14 and CD16 (see STAR Methods); protein levels were not used to construct the trajectory.

(E) Gene expression of select leading-edge genes from pathways enriched (2A) in CD14$^+$ monocytes along pseudotime shows two broad categories of genes. Category 1 genes are perturbed by vaccination with increased expression after vaccination in classical monocytes—the dashed line at pseudotime value of 9.5 denotes the peak of activation. Category 2 genes increase continually across pseudotime and have their highest expression in CD16$^+$ CD14$^-$ non-classical monocytes. The top row shows example genes from each category. The bottom row shows the subset of genes falling into each category from the combined hallmark mTORC1 signaling/hypoxia pathways and Reactome interferon signaling pathways. Gene Ontology (GO) biological process and KEGG pathways enriched in the subset of genes from each pathway and category are listed below. Shading represents the 95% confidence interval of the fitted line.

See also Figure S2.

Please cite this article in press as: Mulè et al., Integrating population and single-cell variations in vaccine responses identifies a naturally adjuvanted human immune setpoint, Immunity (2024), https://doi.org/10.1016/j.immuni.2024.04.009

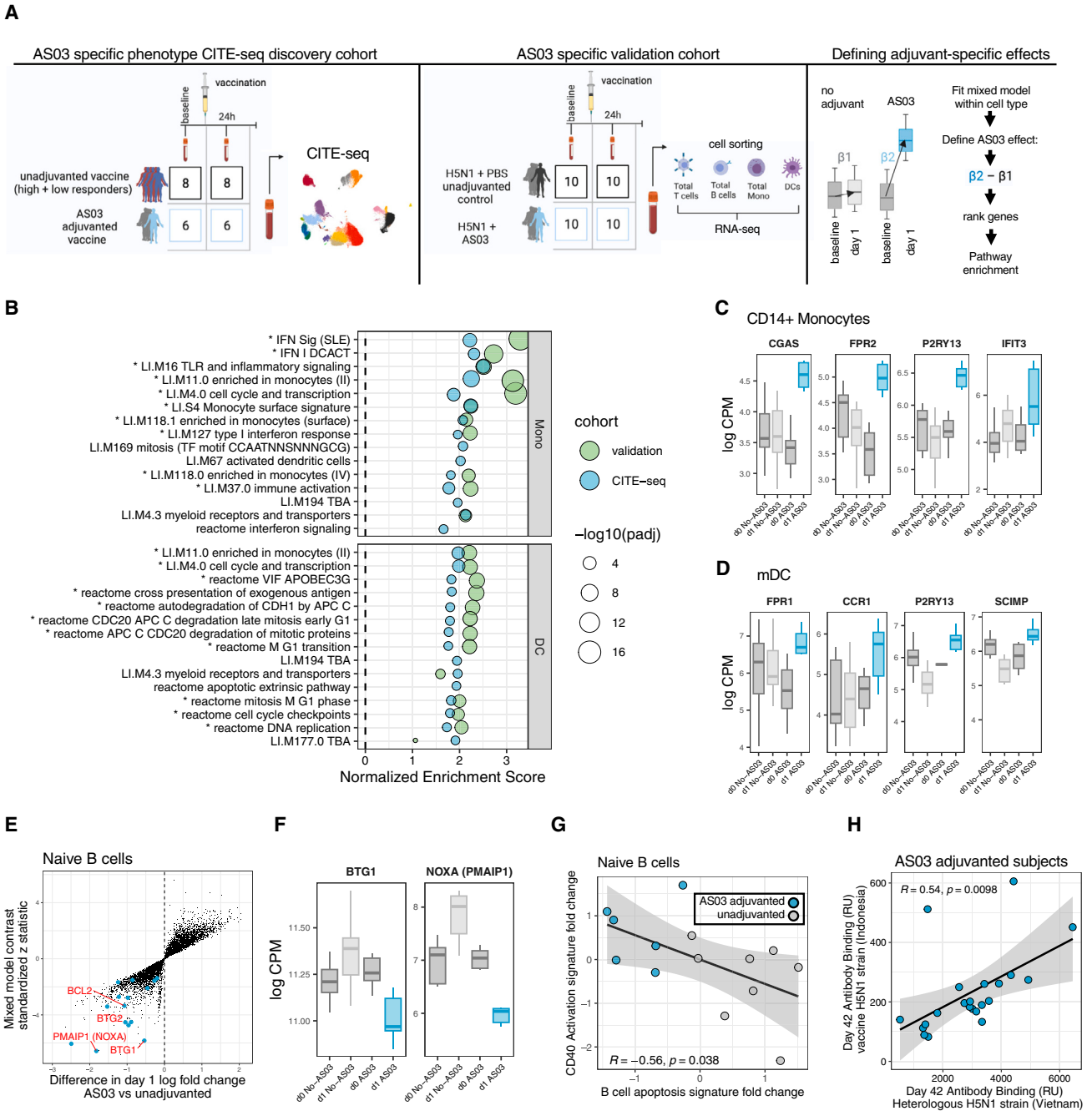

Figure 3. AS03 induces apoptosis suppression signatures in naive B cells and innate-sensing signatures in mDCs and CD14^{+} monocytes

(A) Schematic illustrating the approach we used to define AS03 adjuvant-specific response phenotypes within cell types. Left: unadjuvanted vaccinees were compared with those receiving the H5N1 + AS03-adjuvanted vaccine; surface protein-based cell types are the same as those used in Figure 2; all cells were clustered together for cell type annotation. Middle: data from Howard et al.[60] comparing vaccination with H5N1 + AS03 vs. H5N1 + PBS (control); cell subsets including total T cells, B cells, monocytes, and DCs were sorted based on surface protein markers using FACS followed by RNA sequencing (RNA-seq) analysis at baseline and day 1 following vaccination. Right: statistical contrast/comparison performed within each cell type—genes were fit using a mixed effects model, and the difference in the day 1 fold-change between the AS03-adjuvanted and unadjuvanted groups was calculated within each cell type and visualized with boxplots. Genes were then ranked for gene set enrichment analysis using the effect size of the above contrast that captured AS03-specific responses: gene modules with positive enrichment had higher day 1 fold-change in the AS03 group compared with the group who received the unadjuvanted vaccine.

(B) Gene set enrichment of genes ranked by the procedure outlined in (A) in classical monocytes and mDCs. Results from the CITE-seq data are shown in blue, and those from the validation cohort are in green. All modules/pathways with adjusted p values < 0.05 in the CITE-seq cohort are shown. Pathways with the same direction of enrichment and adjusted p value < 0.01 in the validation cohort are highlighted with an asterisk.

(C) The distribution of log counts per million from aggregated CITE-seq data for each subject showing example genes with AS03-specific responses in CD14^{+} monocytes. Boxplot notches show the median, 25th and 75th percentiles. Individual gene statistics were calculated from the mixed effects model contrast (see

(legend continued on next page)

Please cite this article in press as: Mulè et al., Integrating population and single-cell variations in vaccine responses identifies a naturally adjuvanted human immune setpoint, Immunity (2024), https://doi.org/10.1016/j.immuni.2024.04.009

(Figure 2B). The expression of these genes within classical monocytes alone could cluster samples by time relative to vaccination, suggesting their coordinated induction across individuals after vaccination (Figure 2C).

Inflammatory activation following vaccination was particularly apparent in classical monocytes, such as increases in the level of transcripts in the "IL6 production" pathway, including MYD88, DDX-58 (RIG-I), tumor necrosis factor (TNF), and TRAF6, as well as elevated level of interleukin (IL)-15 and CCL2 transcripts[52] (Figure S2G). Hypoxia and mTORC1 signaling pathway genes were also enriched in classical monocytes (Figure 2A). Although mTOR activity can be subverted to support viral replication,[53] in the context of vaccination, our observation likely reflects the role of mTOR in immune cell activation and inflammation.[54] Indeed, the genes driving this enrichment signal pointed to mTOR-dependent glycolytic metabolism, a process induced after varicella-zoster virus (VZV) vaccination[55] and linked to antigen nonspecific innate memory in monocytes.[56] The mTOR pathway enrichment within $CD25^+$ $CD4^+$ effector T cells, MAIT-like cells, mDCs, and natural killer (NK) cells may have been mediated partly by IL-15 from monocytes in response to the vaccine (Figure S2G), e.g., IL-15 is known to activate mTOR in NK cells.[57] Unadjuvanted influenza vaccine response signatures, including leading-edge driver genes for gene set enrichments, are provided in Table S4.

Integration with pseudotime latent space delineates cellular activation versus differentiation in early vaccination responses

We next explored how time-associated response signatures from our statistical models could be coupled to "bottom-up" computational inference of transcriptional dynamics induced by vaccination in single cells. By using single monocytes from days 0 and 1 samples, we derived a pseudotime, tree-based latent cell-phenotype space by using a "reversed graph embedding" algorithm[58,59] (Figure 2D). CD14 and CD16 surface protein expression patterns identified enrichment of monocyte subsets at the "leaves" of the three tree branches (Figure 2D, bottom margin): pre-vaccination classical monocytes along the left branch, their day 1 counterparts in the top branch, and non-classical monocytes from both pre and post vaccination in the right branch. Integrating the monocyte-specific vaccination response phenotypes from the mixed effects models above (Figure 2A) with this latent space embedding identified two categories of genes based on branch-dependent differential expression (see STAR Methods). Category 1 genes mainly reflected vaccine perturbation effects within $CD14^+$ monocytes (e.g., CCL2), although some were changed in both $CD14^+$ and $CD16^+$ monocytes (e.g., TNFSF10) (Figure 2E, top row). Category 2 genes (e.g., IFITM2 and FCERG1) captured differences and potential differentiation between classical and non-classical monocytes as these genes continuously increased along pseudotime with higher expression in non-classical monocytes, even though vaccination appeared not to induce cellular differentiation between these two subsets (Figure 2E, top row). IFN response genes (Figure 2C) mostly belonged to category 1 (more than 40 genes), except for PTPN1, IFITM2, IFITM3, HLA-C, and EIF4E2, which belonged to category 2. Among genes induced by vaccination in the mTOR and hypoxia pathways, those that belonged to category 2 were enriched for glycolysis processes, while those in category 1 were enriched for ER stress (Figure 2E, bottom). Integrating statistical models defining day 1 changes following vaccination ("real time") and single-cell "pseudotime" delineates cellular activation in response to vaccination versus differences between classical and non-classical monocytes.

AS03 induces specific innate sensing and naive B cell anti-apoptosis signatures

We next examined early responses attributable to the adjuvant AS03. AS03 is known to elicit ~5- to 10-fold greater increases in magnitude and also increased diversity of anti-influenza antibodies compared with unadjuvanted vaccines, even when formulated with a relatively low antigen dose.[35] Previous studies of transcriptional responses to AS03-adjuvanted vaccines revealed strong early induction of ISGs in innate immune cells[35,37,38,60] compared with antigen-only controls. To define early immune response signatures induced specifically by AS03-adjuvanted H5N1 vs. unadjuvanted influenza vaccination, we used similar mixed effects models as above and applied a statistical contrast defining the difference in change from baseline to day 1 between the two vaccines. We further validated these signatures using a publicly available dataset obtained from an independent cohort profiling the transcriptomes of FACS-sorted, major immune cell

STAR Methods): CGAS (also known as MB21D1) standardized z: 3.53, *p* value 4.23e−4; FPR2 standardized z: 5.45, *p* value 4.95e−8; P2RY13 standardized z: 4.93, *p* value 8.13e−7; IFIT3 standardized z: 3.32, *p* value 8.92e−4. Note mixed effects model statistics incorporate observation level weights, covariates, and random effects that are not captured by these boxplots of the log counts per million, which are used here only for visualization and confirmation of the effect. Outliers and lines connecting longitudinal samples from the same subjects not shown to avoid clutter in the visualization.

(D) As in (C), but in mDCs: FPR1 standardized z 2.47, *p* value 0.013; CCR1 standardized z 2.40, *p* value 0.016; P2RY13 standardized z 3.24, *p* value 0.001; SCIMP standardized z 3.74, *p* value 1.88e−4.

(E) Mixed effect modeling results in naive B cells. x axis: difference between AS03-adjuvanted and unadjuvanted vaccination in terms of their log fold-change between days 1 and d0 (baseline); y axis: standardized z statistics of the contrast assessing the same difference using the fitted fixed effect model. Leading-edge genes from the apoptosis signature are highlighted, each with AS03-specific downregulation (NOXA standardized z: −6.57, *p* value: 4.92e−11; BTG1 standardized z: −5.35, *p* value: 5.35e−9).

(F) Boxplot as described in (C) showing the expression distribution of BTG1 and PMAIP1 (NOXA) in log counts per million of aggregated CITE-seq data within naive B cells before and after vaccination.

(G) Scatterplot showing the correlation between the day 1 fold-change in the CD40 activation score and the apoptosis signature in naive B cells. Pearson correlation shown; shading represents the 95% confidence interval of the linear fit.

(H) Scatterplot showing the correlation between antibody avidity to the heterologous strain (x axis, H5N1 Vietnam HA) vs. the vaccine strain (y axis, Indonesia H5N1 HA) measured by surface plasmon resonance assay on day 42 post vaccination in subjects receiving AS03 adjuvant. Pearson correlation shown; shading represents the 95% confidence interval of the linear fit.

See also Figure S3.

Please cite this article in press as: Mulè et al., Integrating population and single-cell variations in vaccine responses identifies a naturally adjuvanted human immune setpoint, Immunity (2024), https://doi.org/10.1016/j.immuni.2024.04.009

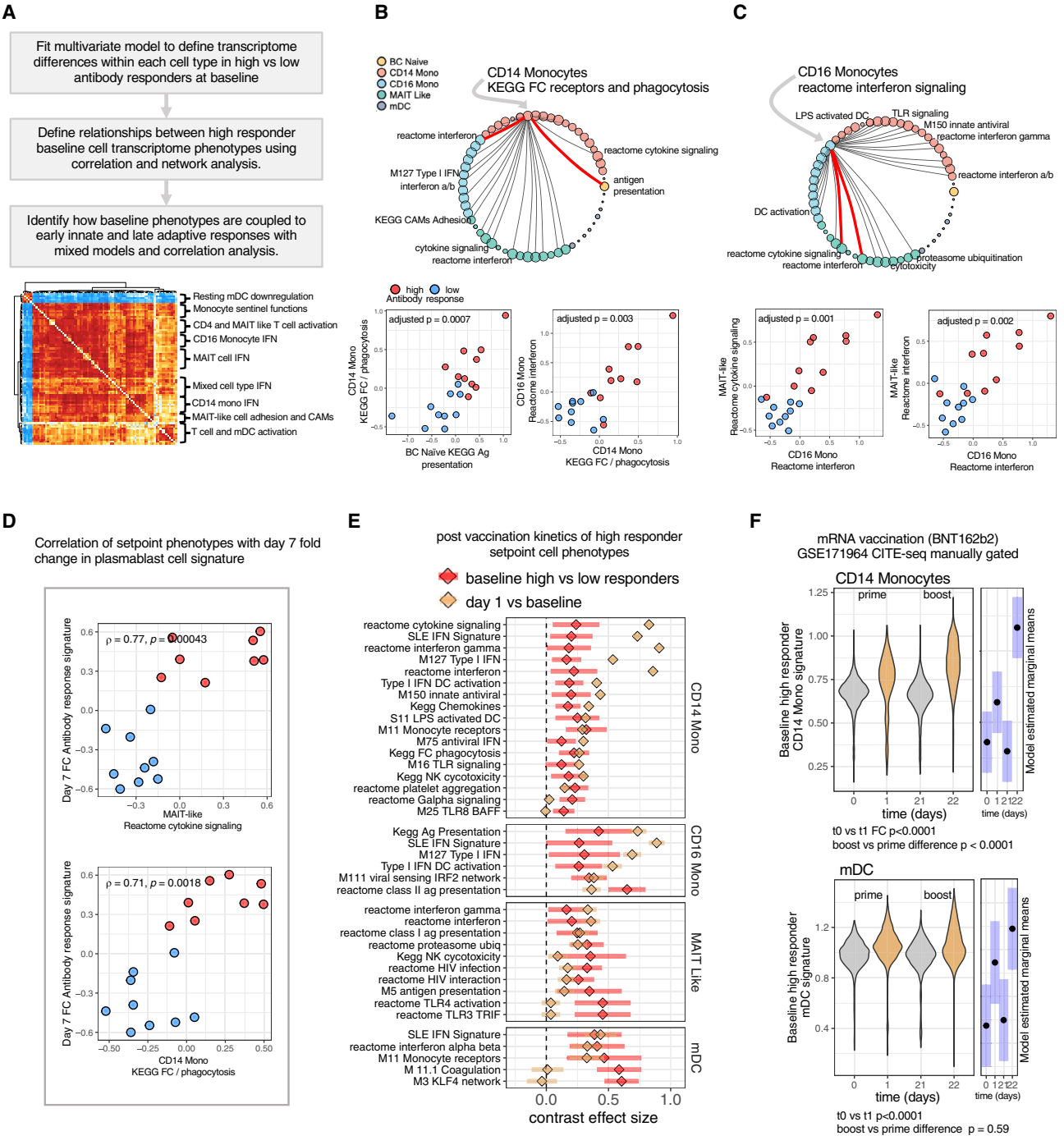

Figure 4. A network of correlated cell-type-specific transcriptional states defines the baseline status of high responders to the unadjuvanted vaccine

(A) Identification of the multicellular baseline high-responder setpoint network. Pathways enriched pre vaccination (baseline) in high vs. low responders within each cell type; genes were ranked using multivariate models adjusting for age, sex, and batch. Leading-edge genes from each cell-type-specific high-responder pathway were correlated across donors within and between cell types. The Jaccard similarity of each pairwise leading-edge gene was subtracted from the Spearman correlation coefficient to correct for correlation due to two signals sharing the same genes only for signals within the same cell type. High connectivity edges were retained in the network (see STAR Methods).

(B and C) Two example highly connected cell phenotypes in the high-responder setpoint network. The edges highlighted in red are shown below as correlations of the activity of the leading-edge genes from those modules across donors within the cell type indicated by the edge. Correlation values reflect Bonferroni adjusted Spearman correlation of phenotypes across the entire network. The size of each vertex (circle size) represents the number of significant connections with that specific signal.

(legend continued on next page)

Please cite this article in press as: Mulè et al., Integrating population and single-cell variations in vaccine responses identifies a naturally adjuvanted human immune setpoint, Immunity (2024), https://doi.org/10.1016/j.immuni.2024.04.009

types (e.g., total B and T cells) of subjects who received the same H5N1 vaccine formulated with either AS03 or PBS, the latter as an unadjuvanted control[60] (Figures 3A and S3A). This analysis revealed positive enrichment of several biological processes more specific to AS03-adjuvanted responses, e.g., those involving surface receptors in monocytes and mDCs (Figure 3B, blue; see schematic in Figure S3A); these were highly concordant with data from similar innate cell subsets in the validation cohort (Figure 3B, green). The leading-edge genes driving these enrichments include receptors recognizing pathogen classes beyond the specific molecular patterns in the vaccine, suggesting AS03 broadly expands the capacity of cells to sense environmental signals. For example, Toll-like receptor (TLR) genes recognizing both bacterial (e.g., TLR1) and viral molecular patterns (e.g., TLR8) were among the leading-edge genes driving the enrichment of module "M16" in $CD14^+$ monocytes, as was FPR2, which can induce chemotaxis in response to bacterial metabolites[61] and cyclic GMP-AMP synthase (CGAS), a cytosolic DNA sensor that activates antiviral responses[62] (Figure 3C). In classical monocytes, three IFN-related pathways were induced by AS03 (Figure 3B); as expected, enrichment of these IFN-related signals was not AS03 specific; it reflected ISG increases beyond the levels seen after unadjuvanted vaccination, as exemplified by IFIT3 (Figure 3C). Within mDCs, a similar pattern of innate cell surface receptors was captured by the enrichment of module "M11" genes, which include inflammatory chemotaxis genes such as FPR1[61] and CCR1,[63] and the proinflammatory TLR adaptor SCIMP. As in $CD14^+$ monocytes, AS03-specific upregulation of P2RY13, an ADP sensor active during inflammation,[64] was also evident in mDCs (Figures 3C and 3D). These observations together suggest that AS03 can enhance the capacity of myeloid cells to sense environmental signals.

Lymphocyte responses by as early as day 1 following vaccination are less well appreciated. We detected a signature suggestive of apoptosis suppression in naive B cells in subjects vaccinated with AS03; this signature included AS03-specific downregulation of genes related to apoptosis including BCL2, BTG2, and NOXA (PMAIP1) 24 h post vaccination (Figures 3E, S3B, and S3C). Further examination of genes with the largest post-vaccination changes in naive B cells revealed an AS03-specific decrease in expression of BTG1, a canonical pro-apoptotic gene. This gene regulates a checkpoint in B cells undergoing germinal center (GC) selection; loss of BTG1 in mice resulted in "supercompetitor" B cells that outcompete their wild-type counterparts within the GC, resulting in aggressive GC-derived lymphomas.[65] Similarly, B cells from $NOXA^{-/-}$ mice outcompeted wild-type cells for entry into the GC following influenza vaccination and infection; these cells persisted longer due to inefficient apoptosis[66] and thus increased the diversity of anti-influenza antibodies.[66] As we and others have shown earlier, AS03 can induce antibodies against influenza clades beyond those in the vaccine.[35,36] Naive B cells of humans after vaccination with AS03 may thus resemble those in $NOXA^{-/-}$ mice after influenza vaccination. Naive B cells from subjects vaccinated with AS03 also appeared more activated based on increased expression of genes linked to CD40 activation,[67,68] and the fold-change in the CD40 activation signature score (day 1/day 0) was negatively correlated with that of an apoptosis signature score in naive B cells (Figure 3G). Both the apoptosis and CD40 activation signatures had consistent directions of change, although apoptosis signature downregulation was not significant in sorted total B cells (pooled naive and memory) in the validation cohort (Figure S3D). Together, these observations suggest that AS03 may function also to suppress apoptosis in naive B lymphocytes early after vaccination to prolong their survival and subsequent activation. The potential increase in the diversity of the naive B cell pool, presumably with varying specificity to vaccine antigens, may help increase the diversity of the subsequent B cell response. The antibody avidity on day 42 against the H5N1 strain in the vaccine was also correlated with that against the non-vaccine strain (Figure 3H), supporting the hypothesis that AS03 may broaden the antibody response by increasing the size of the initial B cell pool available for the GC reaction. Together, our observations highlight two potential mechanisms by which AS03 may drive more robust antibody responses: (1) activation of broad innate-sensing pathways not limited to those specific to the molecular patterns present in the vaccine, and (2) suppression of apoptosis in naive B cells to increase the diversity of naive B cells entering GC reaction with potential positive impacts on antibody response breadth. Detailed information on AS03-specific signatures is provided in Table S4.

Comparing baseline predictive signatures and AS03-specific early responses reveals naturally adjuvanted baseline immune setpoints

We previously described a baseline immune setpoint signature involving multiple cell types predictive of antibody responses to vaccination in healthy individuals and plasma cell-associated disease activity in lupus patients.[22] However, we had focused on a single class of signatures discovered earlier[6] and did not assess how baseline immune status is linked with transcriptional and cellular responses early after vaccination. Here, we first performed unbiased multivariate analysis of CITE-seq data to define baseline immune cell phenotypes associated with antibody response to unadjuvanted vaccination. To understand how baseline phenotypes associated with high responders in

(D) The correlation of signature expression within cell types (x axis) with the day 7 fold-change in microarray data of a signature associated with plasmablast activity that we previously found was predictive of antibody response.
(E) Post-vaccination kinetics of select high-responder setpoint network components. A single-cell mixed effects model of module activity of genes elevated in high vs. low responders was used to estimate the baseline high vs. low responder effect size (red) and subsequent day 1 fold-change across subjects (orange), adjusting for age, sex, cells per donor, and a random effect for donor ID. Bars represent 95% confidence intervals of the estimated marginal means.
(F) Assessing baseline high- vs. low-responder signatures in early (1 day after vaccination) responses to COVID-19 mRNA vaccination (BNT162b2). Day 1 vs. day 0 (dose 1) and day 22 vs. day 21 (dose 2) responses of genes in the baseline high-responder phenotype tested in monocytes and DCs manually gated using CITE-seq data (GEO: GSE171964) obtained from vaccinees. The change of day 1 vs. baseline was statistically significant for both cell types ($p < 0.001$ based on a mixed effect with a subject random effect as in E above). The difference in the fold-change between boost (day 22 vs. day 21) and prime (day 1 vs. day 0) p values: mDC $p = 0.59$, CD14 monocyte $p < 0.001$. Bars represent 95% confidence intervals of the estimated marginal means.
See also Figure S4.

Please cite this article in press as: Mulè et al., Integrating population and single-cell variations in vaccine responses identifies a naturally adjuvanted human immune setpoint, Immunity (2024), https://doi.org/10.1016/j.immuni.2024.04.009

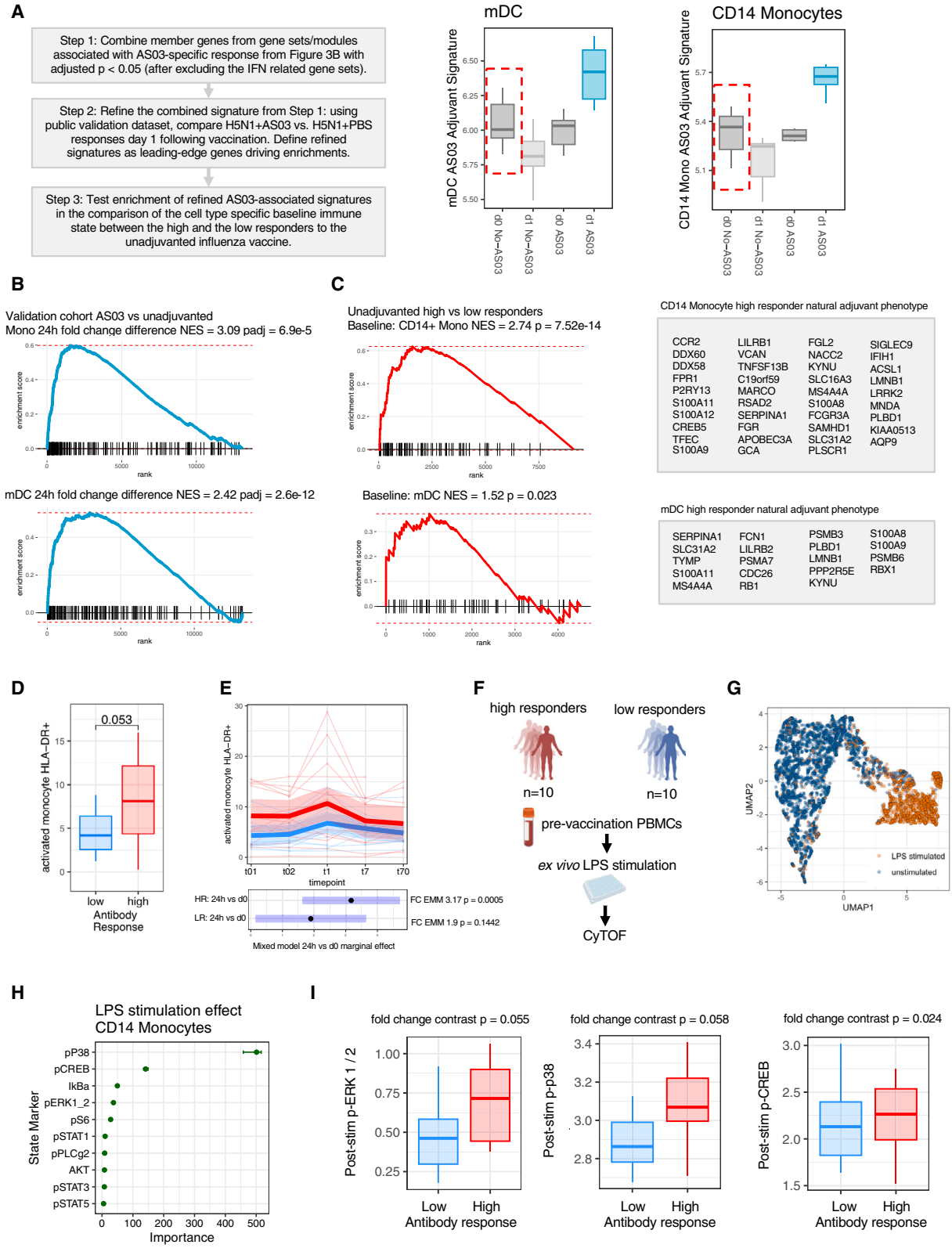

Figure 5. High responders to the unadjuvanted vaccine have a naturally adjuvanted baseline immune setpoint state

(A) Left: outline of the procedure used to assess naturally adjuvanted baseline immune setpoints. The average log counts per million of the combined mDC (middle) and classical monocyte (right) AS03-specific signature genes at baseline (day 0) and day 1 post vaccination (day 1) in unadjuvanted (No-AS03) and

(legend continued on next page)

Please cite this article in press as: Mulè et al., Integrating population and single-cell variations in vaccine responses identifies a naturally adjuvanted human immune setpoint, Immunity (2024), https://doi.org/10.1016/j.immuni.2024.04.009

different cell subsets relate to one another, we used correlation network analysis to reveal that lymphocyte and innate-immune cell phenotypes comprising baseline predictive signatures could be grouped into several functional categories based on their correlation across individuals. Together, 81 baseline setpoint phenotypes (i.e., cell type-gene set combinations) associated with high responders together formed a correlated network of cell-type-specific transcriptional phenotypes (Figures 4A and S4A; Table S4). Interestingly, consistent with the AS03-associated day 1 responses, some phenotypes (or "nodes") that exhibited "hub"-like properties tended to reflect elevated innate cell surface receptor expression in $CD14^+$ monocytes and ISG expression in $CD16^+$ non-classical monocytes at baseline (Figure S4B; see examples highlighted in Figures 4B and 4C). Within $CD14^+$ monocytes, signature genes include Fc receptor genes (e.g., FCGR3A, FCGR1A, and FCGR2A), regulators of cytoskeletal reorganization active during phagocytosis (e.g., PAK1, ARPC5, CFL1, and ARF6), and second messenger signaling molecules (PIP5K1A, PIK3CD, AKT1, MAPK12, and ARPC2). The expression of these signature genes in classical monocytes was correlated with 27 cell phenotypes coordinately elevated in high responders (adjusted $p < 0.05$) (Figure 4B), including antigen presentation genes in naive B cells and ISGs in $CD16^+$ monocytes (Figure 4B, bottom). ISG expression was also elevated in high responders in a variety of other cell types, including $CD161^+$ $CD3^+$ $CD4^-$ $CD8^-$ T cells (referred to hereafter as "MAIT-like") (Figure 4C, bottom), within which IFITM1, IFITM2, ISG15, and IFI6 drove the enrichment of IFN pathways. These baseline phenotypes were also significantly correlated with the day 7 plasmablast signature score in blood (Figure 4D), which predicted antibody responses. Correlated transcriptional phenotypes at baseline, both within and across cell types, are thus associated with the extent of day 7 plasmablast and subsequent antibody increases following vaccination.

Given the resemblance of the baseline setpoint network to the innate signatures induced early following unadjuvanted (without AS03) vaccination (see Figure 2A), we next asked whether specific phenotypes comprising the high-responder setpoint network were induced by vaccination. Indeed, statistical modeling revealed that certain baseline phenotypes elevated in high responders (to the unadjuvanted vaccine) were induced early (day 1) after vaccination in a cell-type-specific manner (Figure 4E). Thus, the baseline immune state of high vaccine responders may mirror early inflammatory responses induced by vaccination to potentially prime early innate responses. Further supporting this idea, aggregated baseline signatures in monocytes and mDCs associated with high responders were also induced 1 day after either dose of BNT162b2 mRNA severe acute respiratory syndrome coronavirus 2 (SARS-CoV-2) vaccination,[69] with greater elevation after the second dose in both cell types (Figure 4F). Given that the lipid nanoparticle carrier in the mRNA vaccine is thought to act as an adjuvant,[70] these results further suggest that our baseline setpoint signatures might have reflected a naturally adjuvanted state that can enhance innate immune response potential prior to stimulation.

To further test the naturally adjuvanted baseline hypothesis, we refined aggregated transcriptome signatures specific to early responses following AS03 in classical monocytes and mDCs. For each cell type, we took the union of leading-edge genes driving the individual gene set enrichments shown in Figure 3B; to prune genes that may not be AS03 specific, we removed the three ISG-related modules induced by both AS03 and the unadjuvanted vaccine in classical monocytes. This process resulted in two aggregated AS03-specific early response signatures, one for each cell type. In aggregate, these genes decreased rather than increased after unadjuvanted influenza vaccination, further demonstrating their AS03 specificity (Figure 5A). We next further refined the signatures by assessing their enrichment in analogous subsets from the validation cohort[60] using the same contrast approach used above (see Figure 3A). Aggregate signatures were significantly enriched (specific to AS03 vs. the PBS control) post vaccination in the validation cohort; we therefore used the leading-edge genes driving the enrichments as our validated AS03-specific $CD14^+$ monocyte and mDC vaccination signatures (Figure 5B).

AS03-adjuvanted vaccinated individuals. As in Figure 3B, distributions are shown for visualization; statistical analysis with multivariate models is shown in (B) and (C).

(B) Assessing the AS03 signatures we derived via gene set enrichment analysis in the validation cohort comparing H5N1 + AS03 vs. H5N1 + PBS vaccination responses on day 1 evaluated in analogous cell types.

(C) Gene set enrichment of the AS03 signatures from (B) (after refinement using signal from the validation data; see STAR Methods and A) in high vs. low responders to the unadjuvanted influenza vaccine in mDC and CD14 monocyte at baseline. Refined AS03 signatures induced specifically on day 1 following AS03-adjuvanted vaccination are enriched among the genes with increased expression in high vs. low responders after adjusting for age, sex, and batch. Specific genes in the leading edge of the high vs. low responder enrichment are shown in the box on the right.

(D) Log cell frequency of $HLA\text{-}DR^+$ classical monocytes (obtained from flow cytometry data) as a percentage of total classical monocytes in high vs. low responders at baseline, p value from a Wilcoxon rank test. Boxplot notches indicate the median, 25^{th} and 75^{th} percentiles.

(E) The frequency of $HLA\text{-}DR^+$ classical monocytes plotted as a function of time points: two baseline time points (t01, t02) and three time points after vaccination (t1, day 1; t7, day 7; and t70, day 70 post vaccination). Shown below are results from a mixed effects model with an interaction term for time and response group. Day 1 vs. day 0 change in the high-responder group: effect size 3.17, p value = 0.0005; in the low responder group: effect size 1.89, p value = 0.14. The difference in estimated marginal day 1 vs. baseline fold-change is not statistically significant between the two groups. Bars represent 95% confidence intervals of the estimated marginal means.

(F) Schematic outlining CyTOF stimulation experiment. PBMCs isolated from high and low responders were stimulated with lipopolysaccharide (LPS). Stimulation phenotype and markers driving stimulation were defined using HDStIM.[71]

(G) UMAP plot of a random subset of 5,000 monocytes pre and post-stimulation with stimulated cells in orange and unstimulated cells in blue.

(H) Variable importance for individual phospho-protein markers used for automatic determination of responding cells reported by HDStIM

(I) The post-stimulation median marker intensity of phosphorylated signaling markers within the $CD14^+$ monocyte cluster-post-stimulation aggregated data shown due to variable baseline phospho-marker detection. Stimulation effects were tested using a mixed model adjusting for batch and modeling individual variation with a random effect for donor ID. The difference in pre- vs. post-stimulation fold-changes in high vs. low responders contrast estimate and p values: p38 contrast effect: 0.104, $p = 0.058$, pCREB contrast effect: 0.223, $p = 0.024$, pERK contrast effect: 0.58, $p = 0.055$.

Please cite this article in press as: Mulè et al., Integrating population and single-cell variations in vaccine responses identifies a naturally adjuvanted human immune setpoint, Immunity (2024), https://doi.org/10.1016/j.immuni.2024.04.009

We tested these AS03-specific signatures in a cell-type-specific manner at baseline in high versus the low responders to the unadjuvanted influenza vaccine. Indeed, each signature was significantly higher in high responders within the corresponding cell type (Figure 5C; Table S1). Thus, innate cell subsets from high responders at baseline resembled AS03-specific day 1 post-vaccination response signatures. An earlier study identified increased frequency of activated HLA-DR$^+$ monocytes 1 day after vaccination.[9] Consistently, here the high responders to the unadjuvanted vaccination already had elevated frequency of HLA-DR$^+$ monocytes[6] at baseline (Figure 5D). Furthermore, by day 1 post vaccination, the frequency of these HLA-DR$^+$ monocyte increased more in high responders (effect size 3.17 for day 1 vs. day 0, p = 0.0005) than low responders (1.89, p = 0.14, respectively) (Figure 5E). Thus, both transcriptional and cell frequency analyses support the conclusion that the baseline immune status of high responders corresponds to a naturally adjuvanted innate immune cell state that mirrors not only the early responses induced by both the unadjuvanted and adjuvanted vaccines (e.g., high ISG status) but also those specifically elicited by the adjuvant AS03.

The naturally adjuvanted baseline state may partly reflect cell-intrinsic response capacity to innate immune cell stimulation. To evaluate this hypothesis, we stimulated pre-vaccination PBMCs from the same 10 high and 10 low unadjuvanted vaccine responders *ex vivo* with IFN alpha, PMA plus ionomycin, and lipopolysaccharide (LPS). We then tested phosphorylation signaling responses 15 min after stimulation to assess whether certain cell subsets were intrinsically more responsive in transducing these external stimulatory signals (Figure 5F). We used cytometry-by-time-of-flight (CyTOF) for cell surface protein and intracellular phosphorylation-based signaling readouts and defined the responding cell populations and associated response markers with a computational algorithm we developed called HDStIM[72] (Figures 5G and 5H). As expected, CD14$^+$ monocytes responded strongly to LPS, as evident by increased phosphorylated p38, CREB, IkBa, and ERK (Figure 5H). The difference in the post LPS-stimulation fold-change of p38, pERK, and pCREB was elevated to a greater extent in high compared with low responders at this early time point (Figure 5I), thus supporting the idea that the naturally adjuvanted baseline set point state reflected elevated cell-intrinsic signaling response capacity. This TLR-dependent increase in the signaling capacity suggests that high responders are poised to mount a stronger response to stimulatory signals from the vaccine, thus resulting in higher downstream transcriptional outputs such as ISGs in both monocytes and DCs, which in turn could trigger autocrine/paracrine circuits to further amplify the response.[73,74] Together, these observations provide additional insights into the mechanistic underpinnings of a naturally adjuvanted human immune setpoint.

DISCUSSION

Here, we introduce a framework for integrating human population variation with multimodal single-cell variation capturing cellular states before and after a perturbation. Analysis of single-cell data often relies on qualitative visualization[75] and univariate analysis, which are inadequate for more complex experiment designs with many samples.[76] By contrast, multilevel models provide a quantitative means to integrate human and single-cell variations to generate new hypotheses and biological insights. Our approach provides a robust framework for complex experimental designs, as exemplified by our CITE-seq data with longitudinal samples from multiple individuals nested into three groups defined by vaccine formulation and responder status. Our analyses revealed novel cell-type-specific phenotypes specifically induced by AS03,[35] including a naive B cell survival signature emerged 1 day after vaccination, suggesting mechanisms by which the AS03 adjuvant may help expand the responding B cell and antibody repertoire.

In addition, we unbiasedly defined the landscape of baseline immune phenotypes linked to high antibody responses to an unadjuvanted influenza vaccine, demonstrating that such baseline states do not merely reflect the phenotypes of a single-cell type but capture a correlated set of phenotypes across multiple cell types, as we had previously shown for a specific baseline signature predictive of antibody responses to vaccination.[22] Furthermore, comparing the baseline cell-type-specific predictors of unadjuvanted vaccine responses with phenotypes induced specifically by the unadjuvanted influenza vaccine, the COVID-19 mRNA vaccine, or the AS03-adjuvanted H5N1 vaccine revealed that high responders to the unadjuvanted vaccine appear to be naturally adjuvanted at baseline. This concept was further buttressed by data comparing phosphoprotein signaling responses to *in vitro* TLR stimulation of baseline cells from high vs. low vaccine responders. These findings advance the concept that modulating baseline setpoints may improve immune response outcomes in diverse contexts.[21] For example, states of clinical immune suppression, e.g., after transplantation or chemotherapy, could be tuned to phenocopy the naturally adjuvanted state we identified in innate immune cells to enhance future vaccination or immunotherapy outcomes.

A host of approaches can be used to tune immune setpoints, including vaccination itself. BCG vaccination has been known to confer nonspecific protection (i.e., not just against TB) and reduce all-cause mortality in infants[77]; it has also been shown to potentiate nonspecific secondary innate immune cell responses in mice.[78] Phase III human trials evaluating BCG vaccination as a nonspecific immunomodulator showed promise in protection against respiratory infections in the elderly,[79] who tend to be immunosuppressed.[45] Future work could quantify the degree to which the naturally adjuvanted phenotype we describe here may relate to innate immune potentiation conferred by BCG vaccination,[80,81] which has been often attributed to chromatin remodeling.[82] In addition, programming the persistence of the naturally adjuvanted baseline setpoint could also be evaluated.

Evaluation of larger cohorts using similar multimodal single-cell approaches will help assess the generalizability of the naturally adjuvanted state we uncovered. In general and supporting our findings, data from multiple vaccination studies revealed substantial inter-subject variation in baseline immune states[1,2,6,83] and a meta-analysis of multiple influenza vaccine studies using blood transcriptomic data revealed an "inflammatory signaling" module predictive of antibody response in subjects under the age of 65.[16] More recent work, based on analysis across different vaccination cohorts, similarly revealed that individuals with an elevated "inflammation" bulk transcriptomic

Please cite this article in press as: Mulè et al., Integrating population and single-cell variations in vaccine responses identifies a naturally adjuvanted human immune setpoint, Immunity (2024), https://doi.org/10.1016/j.immuni.2024.04.009

phenotype tended to have better antibody responses.[23] How age-related inflammation, generally associated with poorer vaccine responses, is similar to or distinct from such baseline inflammatory states is less clear. Earlier work suggests tonic IFN signals in the young are distinct from age-related inflammation related to TNF signaling and its downstream effects.[84,85] Our work provides a framework for future studies to further assess these signatures and concepts at the cell population and single-cell levels.

Limitations of the study

Our study has several limitations. Our comparison of the adjuvanted response with the unadjuvanted response involved different antigens (H5N1 vs. seasonal + 2009pH1N1, respectively). However, we validated signals in an external cohort comparing vaccines with the same H5N1 antigen formulated with AS03 versus a PBS control; additionally, current evidence[86,87] indicates that the H5 antigen-only vaccines have lower (e.g., tens of folds lower in geometric mean[36]) and less durable antibody titers than AS03-adjuvanted formulations (e.g., Link et al.[60] and our own data [unpublished data][36]). An earlier report comparing bulk transcriptomic responses of several AS adjuvant formulations with the hepatitis B antigen[38] also revealed that AS03 induced stronger innate responses, though the bulk transcriptomic data could not pinpoint cell-type-specific responses as we had analyzed here. Together, these data suggest the H5N1 antigen itself has low immunogenicity,[36] and the highly immunogenic responses we observed with the AS03-adjuvanted vaccine were due to the adjuvant and not the antigen. Profiling blood alone omits cells and processes occurring in tissues. Although logistically and clinically more challenging, assessing tissues such as lymph nodes would give a more comprehensive picture of vaccination response variations across individuals, as recent pioneering work using fine needle aspirates or biopsies from lymph nodes had shown.[88–90] For example, our single-cell deconvolution of a day 7 bulk transcriptomic signature predictive of antibody responses confirmed that it originated exclusively from a small number of plasmablast cells. Circulating plasmablasts were shown to share B cell receptor sequences with those obtained from lymph node biopsies[91]; thus, the whole blood plasmablast transcriptional signatures often detected post vaccination most likely originate from lymph nodes, as expected and supported by our results. Determining the tissue origin of the innate immune cells in circulation on day 1 and their connection to circulating cells "encoding" the naturally adjuvanted baseline states remains an open question. Given that monocytes have relatively short half-life, the dynamics and status of the myeloid progenitors need to be considered and may hold a key to linking immune cell status in the bone marrow and shorter-lived circulating cells in blood. Tracking the clonal origins of innate immune cells lacking variable receptor sequences (like in B/T lymphocytes) in humans presents a major challenge. However, recent developments in mitochondrial DNA mutation profiling using single-cell ATAC-seq data could be informative in this context.[92] Another open issue is the origin of the naturally adjuvanted baseline immune state within individuals—what sets the setpoint? Our recent work suggests prior infections can modulate baseline states in humans; months after clinical recovery from mild COVID-19 men and women had a temporally stable but altered baseline immune state compared with matching controls, and men tended to mount more robust innate and adaptive responses to the seasonal influenza vaccine.[27] Future work could assess whether and how the monocyte and DC naturally adjuvanted phenotypes overlap with those stably modified by prior infections in the same cells. Finally, vaccination itself, including BCG and, as recently described, influenza vaccination with adjuvants[93] or even without advjuants (unpublished data), can also potentially modulate baseline immune states.

STAR★METHODS

Detailed methods are provided in the online version of this paper and include the following:

- KEY RESOURCES TABLE
- RESOURCE AVAILABILITY
  - Lead contact
  - Materials availability
  - Data and code availability
- EXPERIMENTAL MODEL AND PARTICIPANT DETAILS
  - Human vaccination comparison cohorts and antibody response assessment
- METHOD DETAILS
  - CITE-seq profiling of peripheral blood mononuclear cells
  - CITE-seq data sequence alignment and sample demultiplexing
  - CyTOF profiling of phospho-signaling responses after stimulation of high and low responder baseline PBMCs
- QUANTIFICATION AND STATISTICAL ANALYSIS
  - Surface protein and mRNA count data normalization
  - Surface protein-based clustering and cell type annotation
  - Hierarchical transcriptome variance deconstruction to infer individual (subject intrinsic), cell type, and vaccine effects
  - Within cell type linear mixed effect models of vaccination effects on gene expression
  - Gene set enrichment testing of vaccination effects within cell types using specific hypothesis-driven gene sets or unbiased analysis
  - Inference of the baseline immune setpoint network
  - Single-cell mixed-effect models of gene expression
  - Software for implementing analysis workflow
  - Monocyte differentiation and perturbation pseudotime analysis
  - Cell frequency analysis
  - Analysis of phospho-signaling responses after stimulation of high and low responder baseline PBMCs using CyTOF

SUPPLEMENTAL INFORMATION

Supplemental information can be found online at https://doi.org/10.1016/j.immuni.2024.04.009.

ACKNOWLEDGMENTS

The authors thank members of the Tsang lab for discussions related to this work and valuable input. This research was supported by the Intramural Research Program of the National Institute of Allergy and Infectious Diseases (NIAID) and the Intramural Programs of the NIH Institutes supporting the Center for Human Immunology. Diagrams in Figures 1A, 3A, 5F, and S3A were created using BioRender.com. We thank Sarah Hopkins for assistance with illustrations. We thank Mani Narayanan for assistance with processing flow cytometry data. We thank Eoin Mckinney, Gosia Trynka, Petter Brodin, Sarah Teichmann, and Ken Smith for constructive comments on this work.

AUTHOR CONTRIBUTIONS

M.P.M., A.J.M., and J.S.T. designed CITE-seq experiments. M.P.M. and A.J.M. generated CITE-seq data and performed pilot experiments with help

Please cite this article in press as: Mulè et al., Integrating population and single-cell variations in vaccine responses identifies a naturally adjuvanted human immune setpoint, Immunity (2024), https://doi.org/10.1016/j.immuni.2024.04.009

from N.B. and A.J. M.P.M. and J.S.T. designed analysis strategies with contributions from A.J.M. M.P.M. analyzed the data, created the scglmmr package, and created the figures with inputs from A.J.M. and J.S.T. F.C. and Y.K. assisted with raw data processing. J.A.Q. and B.A.S. generated the CyTOF data. R.F. developed the HDStIM package and contributed to the analysis of CyTOF data. M.P.M. and J.S.T. interpreted results with contributions from P.L.S. and A.J.M. M.P.M. drafted the manuscript with contributions from A.J.M., P.L.S., and J.S.T. J.S.T. finalized the manuscript and supervised the study.

DECLARATION OF INTERESTS

J.S.T. serves on the Scientific Advisory Boards of CytoReason Inc, Immunoscape, and the Human Immunome Project.

Received: March 28, 2023
Revised: January 21, 2024
Accepted: April 12, 2024
Published: May 1, 2024

REFERENCES

1. Brodin, P., and Davis, M.M. (2017). Human immune system variation. Nat. Rev. Immunol. *17*, 21–29. https://doi.org/10.1038/nri.2016.125.
2. Carr, E.J., Dooley, J., Garcia-Perez, J.E., Lagou, V., Lee, J.C., Wouters, C., Meyts, I., Goris, A., Boeckxstaens, G., Linterman, M.A., et al. (2016). The cellular composition of the human immune system is shaped by age and cohabitation. Nat. Immunol. *17*, 461–468. https://doi.org/10.1038/ni.3371.
3. Liston, A., Humblet-Baron, S., Duffy, D., and Goris, A. (2021). Human immune diversity: from evolution to modernity. Nat. Immunol. *22*, 1479–1489. https://doi.org/10.1038/s41590-021-01058-1.
4. Tsang, J.S. (2015). Utilizing population variation, vaccination, and systems biology to study human immunology. Trends Immunol. *36*, 479–493. https://doi.org/10.1016/j.it.2015.06.005.
5. Pulendran, B., Li, S., and Nakaya, H.I. (2010). Systems Vaccinology. Immunity *33*, 516–529. https://doi.org/10.1016/j.immuni.2010.10.006.
6. Tsang, J.S., Schwartzberg, P.L., Kotliarov, Y., Biancotto, A., Xie, Z., Germain, R.N., Wang, E., Olnes, M.J., Narayanan, M., Golding, H., et al. (2014). Global analyses of human immune variation reveal baseline predictors of postvaccination responses. Cell *157*, 499–513. https://doi.org/10.1016/j.cell.2014.03.031.
7. Nakaya, H.I., Hagan, T., Duraisingham, S.S., Lee, E.K., Kwissa, M., Rouphael, N., Frasca, D., Gersten, M., Mehta, A.K., Gaujoux, R., et al. (2015). Systems Analysis of Immunity to Influenza Vaccination across Multiple Years and in Diverse Populations Reveals Shared Molecular Signatures. Immunity *43*, 1186–1198. https://doi.org/10.1016/j.immuni.2015.11.012.
8. Querec, T.D., Akondy, R.S., Lee, E.K., Cao, W., Nakaya, H.I., Teuwen, D., Pirani, A., Gernert, K., Deng, J., Marzolf, B., et al. (2009). Systems biology approach predicts immunogenicity of the yellow fever vaccine in humans. Nat. Immunol. *10*, 116–125. https://doi.org/10.1038/ni.1688.
9. Sobolev, O., Binda, E., O'Farrell, S., Lorenc, A., Pradines, J., Huang, Y., Duffner, J., Schulz, R., Cason, J., Zambon, M., et al. (2016). Adjuvanted influenza-H1N1 vaccination reveals lymphoid signatures of age-dependent early responses and of clinical adverse events. Nat. Immunol. *17*, 204–213. https://doi.org/10.1038/ni0616-740b.
10. Furman, D., Jojic, V., Kidd, B., Shen-Orr, S., Price, J., Jarrell, J., Tse, T., Huang, H., Lund, P., Maecker, H.T., et al. (2013). Apoptosis and other immune biomarkers predict influenza vaccine responsiveness. Mol. Syst. Biol. *9*, 659. https://doi.org/10.1038/msb.2013.15.
11. Bucasas, K.L., Franco, L.M., Shaw, C.A., Bray, M.S., Wells, J.M., Niño, D., Arden, N., Quarles, J.M., Couch, R.B., and Belmont, J.W. (2011). Early patterns of gene expression correlate with the humoral immune response to influenza vaccination in humans. J. Infect. Dis. *203*, 921–929. https://doi.org/10.1093/infdis/jiq156.
12. Gaucher, D., Therrien, R., Kettaf, N., Angermann, B.R., Boucher, G., Filali-Mouhim, A., Moser, J.M., Mehta, R.S., Drake, D.R., Castro, E., et al. (2008). Yellow fever vaccine induces integrated multilineage and polyfunctional immune responses. J. Exp. Med. *205*, 3119–3131. https://doi.org/10.1084/jem.20082292.
13. Obermoser, G., Presnell, S., Domico, K., Xu, H., Wang, Y., Anguiano, E., Thompson-Snipes, L.A., Ranganathan, R., Zeitner, B., Bjork, A., et al. (2013). Systems scale interactive exploration reveals quantitative and qualitative differences in response to influenza and pneumococcal vaccines. Immunity *38*, 831–844. https://doi.org/10.1016/j.immuni.2012.12.008.
14. Avey, S., Mohanty, S., Chawla, D.G., Meng, H., Bandaranayake, T., Ueda, I., Zapata, H.J., Park, K., Blevins, T.P., Tsang, S., et al. (2020). Seasonal Variability and Shared Molecular Signatures of Inactivated Influenza Vaccination in Young and Older Adults. J. Immunol. *204*, 1661–1673. https://doi.org/10.4049/jimmunol.1900922.
15. Franco, L.M., Bucasas, K.L., Wells, J.M., Niño, D., Wang, X., Zapata, G.E., Arden, N., Renwick, A., Yu, P., Quarles, J.M., et al. (2013). Integrative genomic analysis of the human immune response to influenza vaccination. eLife *2*, e00299. https://doi.org/10.7554/eLife.00299.
16. HIPC-CHI Signatures Project Team; HIPC-I Consortium (2017). Multicohort analysis reveals baseline transcriptional predictors of influenza vaccination responses. Sci. Immunol. *2*, eaal4656. https://doi.org/10.1126/sciimmunol.aal4656.
17. Thakar, J., Mohanty, S., West, A.P., Joshi, S.R., Ueda, I., Wilson, J., Meng, H., Blevins, T.P., Tsang, S., Trentalange, M., et al. (2015). Aging-dependent alterations in gene expression and a mitochondrial signature of responsiveness to human influenza vaccination. Aging *7*, 38–52. https://doi.org/10.18632/aging.100720.
18. Furman, D., Hejblum, B.P., Simon, N., Jojic, V., Dekker, C.L., Thiébaut, R., Tibshirani, R.J., and Davis, M.M. (2014). Systems analysis of sex differences reveals an immunosuppressive role for testosterone in the response to influenza vaccination. Proc. Natl. Acad. Sci. USA *111*, 869–874. https://doi.org/10.1073/pnas.1321060111.
19. Fourati, S., Cristescu, R., Loboda, A., Talla, A., Filali, A., Railkar, R., Schaeffer, A.K., Favre, D., Gagnon, D., Peretz, Y., et al. (2016). Pre-vaccination inflammation and B-cell signalling predict age-related hyporesponse to hepatitis B vaccination. Nat. Commun. *7*, 10369. https://doi.org/10.1038/ncomms10369.
20. Moncunill, G., Carnes, J., Chad Young, W.C., Carpp, L., De Rosa, S., Campo, J.J., Nhabomba, A., Mpina, M., Jairoce, C., Finak, G., et al. (2022). Transcriptional correlates of malaria in RTS,S/AS01-vaccinated African children: A matched case-control study. eLife *11*, 1–30. https://doi.org/10.7554/eLife.70393.
21. Tsang, J.S., Dobaño, C., VanDamme, P., Moncunill, G., Marchant, A., Othman, R.B., Sadarangani, M., Koff, W.C., and Kollmann, T.R. (2020). Improving Vaccine-Induced Immunity: Can Baseline Predict Outcome? Trends Immunol. *41*, 457–465. https://doi.org/10.1016/j.it.2020.04.001.
22. Kotliarov, Y., Sparks, R., Martins, A.J., Mulè, M.P., Lu, Y., Goswami, M., Kardava, L., Banchereau, R., Pascual, V., Biancotto, A., et al. (2020). Broad immune activation underlies shared set point signatures for vaccine responsiveness in healthy individuals and disease activity in patients with lupus. Nat. Med. *26*, 618–629. https://doi.org/10.1038/s41591-020-0769-8.
23. Fourati, S., Tomalin, L.E., Mulè, M.P., Chawla, D.G., Gerritsen, B., Rychkov, D., Henrich, E., Miller, H.E.R., Hagan, T., Diray-Arce, J., et al. (2022). Pan-vaccine analysis reveals innate immune endotypes predictive of antibody responses to vaccination. Nat. Immunol. *23*, 1777–1787. https://doi.org/10.1038/s41590-022-01329-5.
24. Xhonneux, L.P., Knight, O., Lernmark, Å., Bonifacio, E., Hagopian, W.A., Rewers, M.J., She, J.X., Toppari, J., Parikh, H., Smith, K.G.C., et al. (2021). Transcriptional networks in at-risk individuals identify signatures of type 1 diabetes progression. Sci. Transl. Med. *13*, 1–16. https://doi.org/10.1126/scitranslmed.abd5666.

Please cite this article in press as: Mulè et al., Integrating population and single-cell variations in vaccine responses identifies a naturally adjuvanted human immune setpoint, Immunity (2024), https://doi.org/10.1016/j.immuni.2024.04.009

25. Lozano, A.X., Chaudhuri, A.A., Nene, A., Bacchiocchi, A., Earland, N., Vesely, M.D., Usmani, A., Turner, B.E., Steen, C.B., Luca, B.A., et al. (2022). T cell characteristics associated with toxicity to immune checkpoint blockade in patients with melanoma. Nat. Med. *28*, 353–362. https://doi.org/10.1038/s41591-021-01623-z.

26. Zhao, C., Mulè, M.P., Martins, A.J., Pinal-Fernandez, I., Donahue, R.N., Chen, J., Schlom, J., Gulley, J.L., Mammen, A., Tsang, J.S., et al. (2022). Contrasting autoimmune and treatment effects reveals baseline set points of immune toxicity following checkpoint inhibitor treatment. Preprint at bioRxiv. https://doi.org/10.1101/2022.06.05.494592.

27. Sparks, R., Lau, W.W., Liu, C., Han, K.L., Vrindten, K.L., Sun, G., Cox, M., Andrews, S.F., Bansal, N., Failla, L.E., et al. (2023). Influenza vaccination reveals sex dimorphic imprints of prior mild COVID-19. Nature *614*, 752–761. https://doi.org/10.1038/s41586-022-05670-5.

28. Germain, R.N., and Schwartzberg, P.L. (2011). The human condition: An immunological perspective. Nat. Immunol. *12*, 369–372. https://doi.org/10.1038/ni0511-369.

29. Germain, R.N. (2018). Will systems biology deliver its promise and contribute to the development of new or improved vaccines? What really constitutes the study of "systems biology" and how might such an approach facilitate vaccine design. Cold Spring Harb. Perspect. Biol. *10*, a033308. https://doi.org/10.1101/cshperspect.a033308.

30. Lu, Y., Biancotto, A., Cheung, F., Remmers, E., Shah, N., McCoy, J.P., and Tsang, J.S. (2016). Systematic Analysis of Cell-to-Cell Expression Variation of T Lymphocytes in a Human Cohort Identifies Aging and Genetic Associations. Immunity *45*, 1162–1175. https://doi.org/10.1016/j.immuni.2016.10.025.

31. Roederer, M., Quaye, L., Mangino, M., Beddall, M.H., Mahnke, Y., Chattopadhyay, P., Tosi, I., Napolitano, L., Terranova Barberio, M., Menni, C., et al. (2015). The genetic architecture of the human immune system: A bioresource for autoimmunity and disease pathogenesis. Cell *161*, 387–403. https://doi.org/10.1016/j.cell.2015.02.046.

32. Lakshmikanth, T., Muhammad, S.A., Olin, A., Chen, Y., Mikes, J., Fagerberg, L., Gummesson, A., Bergström, G., Uhlen, M., and Brodin, P. (2020). Human Immune System Variation during 1 Year. Cell Rep. *32*, 107923. https://doi.org/10.1016/j.celrep.2020.107923.

33. Stoeckius, M., Hafemeister, C., Stephenson, W., Houck-Loomis, B., Chattopadhyay, P.K., Swerdlow, H., Satija, R., and Smibert, P. (2017). Simultaneous epitope and transcriptome measurement in single cells. Nat. Methods *14*, 865–868. https://doi.org/10.1038/nmeth.4380.

34. Tomalka, J.A., Suthar, M.S., Diamond, M.S., and Sekaly, R.P. (2022). Innate antiviral immunity: how prior exposures can guide future responses. Trends Immunol. *43*, 696–705. https://doi.org/10.1016/j.it.2022.07.001.

35. Garçon, N., Vaughn, D.W., and Didierlaurent, A.M. (2012). Development and evaluation of AS03, an Adjuvant System containing α-tocopherol and squalene in an oil-in-water emulsion. Expert Rev. Vaccines *11*, 349–366. https://doi.org/10.1586/erv.11.192.

36. Khurana, S., Coyle, E.M., Manischewitz, J., King, L.R., Gao, J., Germain, R.N., Schwartzberg, P.L., Tsang, J.S., and Golding, H.; and the CHI Consortium (2018). AS03-adjuvanted H5N1 vaccine promotes antibody diversity and affinity maturation, NAI titers, cross-clade H5N1 neutralization, but not H1N1 cross-subtype neutralization. NPJ Vaccines *3*, 40. https://doi.org/10.1038/s41541-018-0076-2.

37. Howard, L.M., Goll, J.B., Jensen, T.L., Hoek, K.L., Prasad, N., Gelber, C.E., Levy, S.E., Joyce, S., Link, A.J., Creech, C.B., et al. (2019). AS03-adjuvanted H5N1 avian influenza vaccine modulates early innate immune signatures in human peripheral blood mononuclear cells. J. Infect. Dis. *219*, 1786–1798. https://doi.org/10.1093/infdis/jiy721.

38. de Mot, L., Bechtold, V., Bol, V., Callegaro, A., Coccia, M., Essaghir, A., Hasdemir, D., Ulloa-Montoya, F., Siena, E., Smilde, A., et al. (2020). Transcriptional profiles of adjuvanted hepatitis B vaccines display variable interindividual homogeneity but a shared core signature. Sci. Transl. Med. *12*, 1–14. https://doi.org/10.1126/scitranslmed.aay8618.

39. Mulè, M.P., Martins, A.J., and Tsang, J.S. (2022). Normalizing and denoising protein expression data from droplet-based single cell profiling. Nat. Commun. *13*, 2099. https://doi.org/10.1038/s41467-022-29356-8.

40. Ellebedy, A.H., Jackson, K.J.L., Kissick, H.T., Nakaya, H.I., Davis, C.W., Roskin, K.M., McElroy, A.K., Oshansky, C.M., Elbein, R., Thomas, S., et al. (2016). Defining antigen-specific plasmablast and memory B cell subsets in human blood after viral infection or vaccination. Nat. Immunol. *17*, 1226–1234. https://doi.org/10.1038/ni.3533.

41. GTEx Consortium (2015). Human genomics. The Genotype-Tissue Expression (GTEx) pilot analysis: Multitissue gene regulation in humans. Science *348*, 648–660. https://doi.org/10.1126/science.1262110.

42. Uhlen, M., Karlsson, M.J., Zhong, W., Tebani, A., Pou, C., Mikes, J., Lakshmikanth, T., Forsström, B., Edfors, F., Odeberg, J., et al. (2019). A genome-wide transcriptomic analysis of protein-coding genes in human blood cells. Science *366*, eaax9198. https://doi.org/10.1126/science.aax9198.

43. Chang, W.C., Jan Wu, Y.J.J., Chung, W.H., Lee, Y.S., Chin, S.W., Chen, T.J., Chang, Y.S., Chen, D.Y., and Hung, S.I. (2017). Genetic variants of PPAR-gamma coactivator 1B augment NLRP3-mediated inflammation in gouty arthritis. Rheumatology (Oxford) *56*, 457–466. https://doi.org/10.1093/rheumatology/kew337.

44. Segovia, M., Russo, S., Jeldres, M., Mahmoud, Y.D., Perez, V., Duhalde, M., Charnet, P., Rousset, M., Victoria, S., Veigas, F., et al. (2019). Targeting TMEM176B Enhances Antitumor Immunity and Augments the Efficacy of Immune Checkpoint Blockers by Unleashing Inflammasome Activation. Cancer Cell *35*, 767–781.e6. https://doi.org/10.1016/j.ccell.2019.04.003.

45. Ferrucci, L., and Fabbri, E. (2018). Inflammageing: chronic inflammation in ageing, cardiovascular disease, and frailty. Nat. Rev. Cardiol. *15*, 505–522. https://doi.org/10.1038/s41569-018-0064-2.

46. Hagan, T., Gerritsen, B., Tomalin, L.E., Fourati, S., Mulè, M.P., Chawla, D.G., Rychkov, D., Henrich, E., Miller, H.E.R., Diray-Arce, J., et al. (2022). Transcriptional atlas of the human immune response to 13 vaccines reveals a common predictor of vaccine-induced antibody responses. Nat. Immunol. *23*, 1788–1798. https://doi.org/10.1038/s41590-022-01328-6.

47. Nakaya, H.I., Wrammert, J., Lee, E.K., Racioppi, L., Marie-Kunze, S., Haining, W.N., Means, A.R., Kasturi, S.P., Khan, N., Li, G.M., et al. (2011). Systems biology of vaccination for seasonal influenza in humans. Nat. Immunol. *12*, 786–795. https://doi.org/10.1038/ni.2067.

48. Nordmann, A., Wixler, L., Boergeling, Y., Wixler, V., and Ludwig, S. (2012). A new splice variant of the human guanylate-binding protein 3 mediates anti-influenza activity through inhibition of viral transcription and replication. FASEB J. *26*, 1290–1300. https://doi.org/10.1096/fj.11-189886.

49. Hsiang, T.Y., Zhao, C., and Krug, R.M. (2009). Interferon-Induced ISG15 Conjugation Inhibits Influenza A Virus Gene Expression and Replication in Human Cells. J. Virol. *83*, 5971–5977. https://doi.org/10.1128/JVI.01667-08.

50. Li, Y., Banerjee, S., Wang, Y., Goldstein, S.A., Dong, B., Gaughan, C., Silverman, R.H., and Weiss, S.R. (2016). Activation of RNase L is dependent on OAS3 expression during infection with diverse human viruses. Proc. Natl. Acad. Sci. USA *113*, 2241–2246. https://doi.org/10.1073/pnas.1519657113.

51. Qu, H., Li, J., Yang, L., Sun, L., Liu, W., and He, H. (2016). Influenza A Virus-induced expression of ISG20 inhibits viral replication by interacting with nucleoprotein. Virus Genes *52*, 759–767. https://doi.org/10.1007/s11262-016-1366-2.

52. Fantuzzi, L., Borghi, P., Ciolli, V., Pavlakis, G., Belardelli, F., and Gessani, S. (1999). Loss of CCR2 Expression and Functional Response to Monocyte Chemotactic Protein (MCP-1) During the Differentiation of Human Monocytes: Role of Secreted MCP-1 in the Regulation of the Chemotactic Response. Blood *94*, 875–883. https://doi.org/10.1182/blood.V94.3.875.415k28_875_883.

Please cite this article in press as: Mulè et al., Integrating population and single-cell variations in vaccine responses identifies a naturally adjuvanted human immune setpoint, Immunity (2024), https://doi.org/10.1016/j.immuni.2024.04.009

53. Kuss-Duerkop, S.K., Wang, J., Mena, I., White, K., Metreveli, G., Sakthivel, R., Mata, M.A., Muñoz-Moreno, R., Chen, X., Krammer, F., et al. (2017). Influenza virus differentially activates mTORC1 and mTORC2 signaling to maximize late stage replication. PLoS Pathog. *13*, e1006635. https://doi.org/10.1371/journal.ppat.1006635.

54. Weichhart, T., Costantino, G., Poglitsch, M., Rosner, M., Zeyda, M., Stuhlmeier, K.M., Kolbe, T., Stulnig, T.M., Hörl, W.H., Hengstschläger, M., et al. (2008). The TSC-mTOR Signaling Pathway Regulates the Innate Inflammatory Response. Immunity *29*, 565–577. https://doi.org/10.1016/j.immuni.2008.08.012.

55. Li, S., Sullivan, N.L., Rouphael, N., Yu, T., Banton, S., Maddur, M.S., McCausland, M., Chiu, C., Canniff, J., Dubey, S., et al. (2017). Metabolic Phenotypes of Response to Vaccination in Humans. Cell *169*, 862–877.e17. https://doi.org/10.1016/j.cell.2017.04.026.

56. Cheng, S.C., Quintin, J., Cramer, R.A., Shepardson, K.M., Saeed, S., Kumar, V., Giamarellos-Bourboulis, E.J., Martens, J.H.A., Rao, N.A., Aghajanirefah, A., et al. (2014). mTOR- and HIF-1α–mediated aerobic glycolysis as metabolic basis for trained immunity. Science *345*, 1250684. https://doi.org/10.1126/science.1250684.

57. Marçais, A., Cherfils-Vicini, J., Viant, C., Degouve, S., Viel, S., Fenis, A., Rabilloud, J., Mayol, K., Tavares, A., Bienvenu, J., et al. (2014). The metabolic checkpoint kinase mTOR is essential for IL-15 signaling during the development and activation of NK cells. Nat. Immunol. *15*, 749–757. https://doi.org/10.1038/ni.2936.

58. Mao, Q., Wang, L., Tsang, I.W., and Sun, Y. (2017). Principal Graph and Structure Learning Based on Reversed Graph Embedding. IEEE Trans. Pattern Anal. Mach. Intell. *39*, 2227–2241. https://doi.org/10.1109/TPAMI.2016.2635657.

59. Qiu, X., Mao, Q., Tang, Y., Wang, L., Chawla, R., Pliner, H.A., and Trapnell, C. (2017). Reversed graph embedding resolves complex single-cell trajectories. Nat. Methods *14*, 979–982. https://doi.org/10.1038/nmeth.4402.

60. Howard, L.M., Hoek, K.L., Goll, J.B., Samir, P., Galassie, A., Allos, T.M., Niu, X., Gordy, L.E., Creech, C.B., Prasad, N., et al. (2017). Cell-based systems biology analysis of human AS03-adjuvanted H5N1 avian influenza vaccine responses: A phase i randomized controlled trial. PLoS One *12*, e0167488. https://doi.org/10.1371/journal.pone.0167488.

61. Bloes, D.A., Kretschmer, D., and Peschel, A. (2015). Enemy attraction: Bacterial agonists for leukocyte chemotaxis receptors. Nat. Rev. Microbiol. *13*, 95–104. https://doi.org/10.1038/nrmicro3390.

62. Sun, L., Wu, J., Du, F., Chen, X., and Chen, Z.J. (2013). Cyclic GMP-AMP synthase is a cytosolic DNA sensor that activates the type I interferon pathway. Science *339*, 786–791. https://doi.org/10.1126/science.1232458.

63. Sallusto, F., Schaerli, P., Loetscher, P., Schaniel, C., Lenig, D., Mackay, C.R., Qin, S., and Lanzavecchia, A. (1998). Rapid and coordinated switch in chemokine receptor expression during dendritic cell maturation. Eur. J. Immunol. *28*, 2760–2769. https://doi.org/10.1002/(SICI)1521-4141(199809)28:09<2760::AID-IMMU2760>3.0.CO;2-N.

64. Chhatbar, C., and Prinz, M. (2021). The roles of microglia in viral encephalitis: from sensome to therapeutic targeting. Cell. Mol. Immunol. *18*, 250–258. https://doi.org/10.1038/s41423-020-00620-5.

65. Mlynarczyk, C., Teater, M., Pae, J., Chin, C.R., Wang, L., Arulraj, T., Barisic, D., Papin, A., Hoehn, K.B., Kots, E., et al. (2023). BTG1 mutation yields supercompetitive B cells primed for malignant transformation. Science *379*, eabj7412. https://doi.org/10.1126/science.abj7412.

66. Wensveen, F.M., Derks, I.A.M., Van Gisbergen, K.P.J.M., De Bruin, A.M., Meijers, J.C.M., Yigittop, H.A., Nolte, M.A., Eldering, E., and Van Lier, R.A.W. (2012). BH3-only protein Noxa regulates apoptosis in activated B cells and controls high-affinity antibody formation. Blood *119*, 1440–1449. https://doi.org/10.1182/blood-2011-09-378877.

67. Gricks, C.S., Zahrieh, D., Zauls, A.J., Gorgun, G., Drandi, D., Mauerer, K., Neuberg, D., and Gribben, J.G. (2004). Differential regulation of gene expression following CD40 activation of leukemic compared to healthy B cells. Blood *104*, 4002–4009. https://doi.org/10.1182/blood-2004-02-0494.

68. Shimabukuro-Vornhagen, A., Zoghi, S., Liebig, T.M., Wennhold, K., Chemitz, J., Draube, A., Kochanek, M., Blaschke, F., Pallasch, C., Holtick, U., et al. (2014). Inhibition of Protein Geranylgeranylation Specifically Interferes with CD40-Dependent B Cell Activation, Resulting in a Reduced Capacity To Induce T Cell Immunity. J. Immunol. *193*, 5294–5305. https://doi.org/10.4049/jimmunol.1203436.

69. Arunachalam, P.S., Scott, M.K.D., Hagan, T., Li, C., Feng, Y., Wimmers, F., Grigoryan, L., Trisal, M., Edara, V.V., Lai, L., et al. (2021). Systems vaccinology of the BNT162b2 mRNA vaccine in humans. Nature *596*, 410–416. https://doi.org/10.1038/s41586-021-03791-x.

70. Hogan, M.J., and Pardi, N. (2022). MRNA Vaccines in the COVID-19 Pandemic and Beyond. Annu. Rev. Med. *73*, 17–39. https://doi.org/10.1146/annurev-med-042420-112725.

71. Farmer, R., Apps, R., and Tsang, J.S. (2022). HDStIM: High Dimensional Stimulation Immune Mapping. https://cran.r-project.org/web/packages/HDStIM/HDStIM.pdf.

72. Farmer, R., Apps, R., Quiel, J., Sellers, B.A., Cheung, F., Chen, J., Mukherjee, A., McGuire, P.J., and Tsang, J.S. (2022). Multiparameter stimulation mapping of signaling states in single pediatric immune cells reveals heightened tonic activation during puberty. Preprint at bioRxiv. https://doi.org/10.1101/2022.11.14.516371.

73. Doyle, S.E., Vaidya, S.A., O'Connell, R., Dadgostar, H., Dempsey, P.W., Wu, T.-T., Rao, G., Sun, R., Haberland, M.E., Modlin, R.L., et al. (2002). IRF3 Mediates a TLR3/TLR4-Specific Antiviral Gene Program. Immunity *17*, 251–263. https://doi.org/10.1016/S1074-7613(02)00390-4.

74. Kawasaki, T., and Kawai, T. (2014). Toll-like receptor signaling pathways. Front. Immunol. *5*, 461. https://doi.org/10.3389/fimmu.2014.00461.

75. Chari, T., and Pachter, L. (2023). The Specious Art of Single-Cell Genomics. PLoS Comput. Biol. *19*, e1011288. https://doi.org/10.1371/journal.pcbi.1011288.

76. Zimmerman, K.D., Espeland, M.A., and Langefeld, C.D. (2021). A practical solution to pseudoreplication bias in single-cell studies. Nat. Commun. *12*, 738. https://doi.org/10.1038/s41467-021-21038-1.

77. Aaby, P., Netea, M.G., and Benn, C.S. (2023). Beneficial non-specific effects of live vaccines against COVID-19 and other unrelated infections. Lancet Infect. Dis. *23*, e34–e42. https://doi.org/10.1016/S1473-3099(22)00498-4.

78. Old, L.J., Clarke, D.A., and Benacerraf, B. (1959). Effect of Bacillus Calmette-Guérin Infection on Transplanted Tumours in the Mouse. Nature *184* (*Suppl 5*), 291–292. https://doi.org/10.1038/184291a0.

79. Giamarellos-Bourboulis, E.J., Tsilika, M., Moorlag, S., Antonakos, N., Kotsaki, A., Domínguez-Andrés, J., Kyriazopoulou, E., Gkavogianni, T., Adami, M.E., Damoraki, G., et al. (2020). Activate: Randomized Clinical Trial of BCG Vaccination against Infection in the Elderly. Cell *183*, 315–323.e9. https://doi.org/10.1016/j.cell.2020.08.051.

80. Netea, M.G., Domínguez-Andrés, J., Barreiro, L.B., Chavakis, T., Divangahi, M., Fuchs, E., Joosten, L.A.B., van der Meer, J.W.M., Mhlanga, M.M., Mulder, W.J.M., et al. (2020). Defining trained immunity and its role in health and disease. Nat. Rev. Immunol. *20*, 375–388. https://doi.org/10.1038/s41577-020-0285-6.

81. Boraschi, D., and Italiani, P. (2018). Innate Immune Memory: Time for Adopting a Correct Terminology. Front. Immunol. *9*, 799. https://doi.org/10.3389/fimmu.2018.00799.

82. Foster, S.L., Hargreaves, D.C., and Medzhitov, R. (2007). Gene-specific control of inflammation by TLR-induced chromatin modifications. Nature *447*, 972–978. https://doi.org/10.1038/nature05836.

83. Brodin, P., Jojic, V., Gao, T., Bhattacharya, S., Angel, C.J.L., Furman, D., Shen-Orr, S., Dekker, C.L., Swan, G.E., Butte, A.J., et al. (2015). Variation in the Human Immune System Is Largely Driven by Non-Heritable Influences. Cell *160*, 37–47. https://doi.org/10.1016/j.cell.2014.12.020.

84. Furman, D., Jojic, V., Sharma, S., Shen-Orr, S.S., Angel, C.J.L., Onengut-Gumuscu, S., Kidd, B.A., Maecker, H.T., Concannon, P., Dekker, C.L., et al. (2015). Cytomegalovirus infection enhances the immune response

Please cite this article in press as: Mulè et al., Integrating population and single-cell variations in vaccine responses identifies a naturally adjuvanted human immune setpoint, Immunity (2024), https://doi.org/10.1016/j.immuni.2024.04.009

to influenza. Sci. Transl. Med. *7*, 281ra43. https://doi.org/10.1126/scitranslmed.aaa2293.

85. Weinberger, B., Haks, M.C., de Paus, R.A., Ottenhoff, T.H.M., Bauer, T., and Grubeck-Loebenstein, B. (2018). Impaired Immune Response to Primary but Not to Booster Vaccination Against Hepatitis B in Older Adults. Front. Immunol. *9*, 1035. https://doi.org/10.3389/fimmu.2018.01035.
86. Langley, J.M., Frenette, L., Ferguson, L., Riff, D., Sheldon, E., Risi, G., Johnson, C., Li, P., Kenney, R., Innis, B., et al. (2010). Safety and Cross-Reactive Immunogenicity of Candidate AS03-Adjuvanted Prepandemic H5N1 Influenza Vaccines: A Randomized Controlled Phase 1/2 Trial in Adults. J. Infect. Dis. *201*, 1644–1653. https://doi.org/10.1086/652701.
87. Langley, J.M., Risi, G., Caldwell, M., Gilderman, L., Berwald, B., Fogarty, C., Poling, T., Riff, D., Baron, M., Frenette, L., et al. (2011). Dose-Sparing H5N1 A/Indonesia/05/2005 Pre-pandemic Influenza Vaccine in Adults and Elderly Adults: A Phase III, Placebo-Controlled, Randomized Study. J. Infect. Dis. *203*, 1729–1738. https://doi.org/10.1093/infdis/jir172.
88. Austin, J.W., Buckner, C.M., Kardava, L., Wang, W., Zhang, X., Melson, V.A., Swanson, R.G., Martins, A.J., Zhou, J.Q., Hoehn, K.B., et al. (2019). Overexpression of T-bet in HIV infection is associated with accumulation of B cells outside germinal centers and poor affinity maturation. Sci. Transl. Med. *11*, eaax0904. https://doi.org/10.1126/scitranslmed.aax0904.
89. Havenar-Daughton, C., Newton, I.G., Zare, S.Y., Reiss, S.M., Schwan, B., Suh, M.J., Hasteh, F., Levi, G., and Crotty, S. (2020). Normal human lymph node T follicular helper cells and germinal center B cells accessed via fine needle aspirations. J. Immunol. Methods *479*, 112746. https://doi.org/10.1016/j.jim.2020.112746.
90. Patricia D'Souza, M., Allen, M.A., Baumblatt, J.A.G., Boggiano, C., Crotty, S., Grady, C., Havenar-Daughton, C., Heit, A., Hu, D.J., Kunwar, N., et al. (2018). Innovative approaches to track lymph node germinal center responses to evaluate development of broadly neutralizing antibodies in human HIV vaccine trials. Vaccine *36*, 5671–5677. https://doi.org/10.1016/j.vaccine.2018.07.071.
91. Turner, J.S., Zhou, J.Q., Han, J., Schmitz, A.J., Rizk, A.A., Alsoussi, W.B., Lei, T., Amor, M., McIntire, K.M., Meade, P., et al. (2020). Human germinal centres engage memory and naive B cells after influenza vaccination. Nature *586*, 127–132. https://doi.org/10.1038/s41586-020-2711-0.
92. Lareau, C.A., Ludwig, L.S., Muus, C., Gohil, S.H., Zhao, T., Chiang, Z., Pelka, K., Verboon, J.M., Luo, W., Christian, E., et al. (2021). Massively parallel single-cell mitochondrial DNA genotyping and chromatin profiling. Nat. Biotechnol. *39*, 451–461. https://doi.org/10.1038/s41587-020-0645-6.
93. Wimmers, F., Donato, M., Kuo, A., Ashuach, T., Gupta, S., Li, C., Dvorak, M., Foecke, M.H., Chang, S.E., Hagan, T., et al. (2021). The single-cell epigenomic and transcriptional landscape of immunity to influenza vaccination. Cell *184*, 3915–3935.e21. https://doi.org/10.1016/j.cell.2021.05.039.
94. Wickham, H., Averick, M., Bryan, J., Chang, W., McGowan, L., François, R., Grolemund, G., Hayes, A., Henry, L., Hester, J., et al. (2019). Welcome to the Tidyverse. J. Open Source Software *4*, 1686. https://doi.org/10.21105/joss.01686.
95. Bates, D., Mächler, M., Bolker, B.M., and Walker, S.C. (2015). Fitting linear mixed-effects models using lme4. J. Stat. Softw. *67*, 1–48. https://doi.org/10.18637/jss.v067.i01.
96. Ritchie, M.E., Phipson, B., Wu, D., Hu, Y., Law, C.W., Shi, W., and Smyth, G.K. (2015). Limma powers differential expression analyses for RNA-sequencing and microarray studies. Nucleic Acids Res. *43*, e47. https://doi.org/10.1093/nar/gkv007.
97. Korotkevich, G., Sukhov, V., and Sergushichev, A. (2019). Fast gene set enrichment analysis. Preprint at bioRxiv. https://doi.org/10.1101/060012.
98. Butler, A., Hoffman, P., Smibert, P., Papalexi, E., and Satija, R. (2018). Integrating single-cell transcriptomic data across different conditions, technologies, and species. Nat. Biotechnol. *36*, 411–420. https://doi.org/10.1038/nbt.4096.
99. McGinnis, C.S., Patterson, D.M., Winkler, J., Conrad, D.N., Hein, M.Y., Srivastava, V., Hu, J.L., Murrow, L.M., Weissman, J.S., Werb, Z., et al. (2019). MULTI-seq: sample multiplexing for single-cell RNA sequencing using lipid-tagged indices. Nat. Methods *16*, 619–626. https://doi.org/10.1038/s41592-019-0433-8.
100. Kang, H.M., Subramaniam, M., Targ, S., Nguyen, M., Maliskova, L., McCarthy, E., Wan, E., Wong, S., Byrnes, L., Lanata, C.M., et al. (2018). Multiplexed droplet single-cell RNA-sequencing using natural genetic variation. Nat. Biotechnol. *36*, 89–94. https://doi.org/10.1038/nbt.4042.
101. Stoeckius, M., Zheng, S., Houck-Loomis, B., Hao, S., Yeung, B.Z., Mauck, W.M., Smibert, P., and Satija, R. (2018). Cell Hashing with barcoded antibodies enables multiplexing and doublet detection for single cell genomics. Genome Biol. *19*, 224. https://doi.org/10.1186/s13059-018-1603-1.
102. McCarthy, D.J., Campbell, K.R., Lun, A.T.L., and Wills, Q.F. (2017). Scater: Pre-processing, quality control, normalization and visualization of single-cell RNA-seq data in R. Bioinformatics *33*, 1179–1186. https://doi.org/10.1093/bioinformatics/btw777.
103. Fernandez, R., and Maecker, H. (2015). Cytokine-stimulated Phosphoflow of PBMC Using CyTOF Mass Cytometry. Bio Protoc. *5*, 5. https://doi.org/10.21769/BioProtoc.1496.
104. Lun, A.T.L., Bach, K., and Marioni, J.C. (2016). Pooling across cells to normalize single-cell RNA sequencing data with many zero counts. Genome Biol. *17*, 75. https://doi.org/10.1186/s13059-016-0947-7.
105. Waltman, L., and Van Eck, N.J. (2013). A smart local moving algorithm for large-scale modularity-based community detection. Eur. Phys. J. B *86*. https://doi.org/10.1140/epjb/e2013-40829-0.
106. Hoffman, G.E., and Schadt, E.E. (2016). variancePartition: Interpreting drivers of variation in complex gene expression studies. BMC Bioinformatics *17*, 483. https://doi.org/10.1186/s12859-016-1323-z.
107. Law, C.W., Chen, Y., Shi, W., and Smyth, G.K. (2014). Voom: Precision weights unlock linear model analysis tools for RNA-seq read counts. Genome Biol. *15*, R29. https://doi.org/10.1186/gb-2014-15-2-r29.
108. Hoffman, G.E., and Roussos, P. (2021). Dream: Powerful differential expression analysis for repeated measures designs. Bioinformatics *37*, 192–201. https://doi.org/10.1093/bioinformatics/btaa687.
109. Hoffman, G.E., Lee, D., Bendl, J., Fnu, P., Hong, A., Casey, C., Alvia, M., Shao, Z., Argyriou, S., Therrien, K., et al. (2023). Efficient differential expression analysis of large-scale single cell transcriptomics data using dreamlet. Preprint at bioRxiv. https://doi.org/10.1101/2023.03.17.533005.
110. Robinson, M.D., McCarthy, D.J., and Smyth, G.K. (2010). edgeR: A Bioconductor package for differential expression analysis of digital gene expression data. Bioinformatics *26*, 139–140. https://doi.org/10.1093/bioinformatics/btp616.
111. Li, S., Rouphael, N., Duraisingham, S., Romero-Steiner, S., Presnell, S., Davis, C., Schmidt, D.S., Johnson, S.E., Milton, A., Rajam, G., et al. (2014). Molecular signatures of antibody responses derived from a systems biology study of five human vaccines. Nat. Immunol. *15*, 195–204. https://doi.org/10.1038/ni.2789.
112. Chen, E.Y., Tan, C.M., Kou, Y., Duan, Q., Wang, Z., Meirelles, G.V., Clark, N.R., and Ma'ayan, A. (2013). Enrichr: interactive and collaborative HTML5 gene list enrichment analysis tool. BMC Bioinformatics *14*, 128. https://doi.org/10.1186/1471-2105-14-128.
113. Lenth, R.V., Bolker, B., Buerkner, P., Giné-Vázquez, I., Herve, M., Jung, M., Love, J., Miguez, F., Riebl, H., and Singmann, H. (2024). emmeans: Estimated Marginal Means, aka Least-Squares Means. R package version 1.8.5. https://CRAN.R-project.org/package=emmeans.

Please cite this article in press as: Mulè et al., Integrating population and single-cell variations in vaccine responses identifies a naturally adjuvanted human immune setpoint, Immunity (2024), https://doi.org/10.1016/j.immuni.2024.04.009

STAR★METHODS

KEY RESOURCES TABLE

REAGENT or RESOURCE	SOURCE	IDENTIFIER
Antibodies		
TotalSeq-A Custom human antibody panel	Biolegend	See Table S5
CyTOF custom human antibody panel	Biolegend, Fluidigm, Novus Biology	
Biological samples		
Human PBMC samples	NIH Protocol 09-H-0239	NA
Human PBMC samples	NIH Protocol 12-H-0103	NA
Critical commercial assays		
Chromium V2 library construction kit	10x Genomics	PN-120237
Hiseq 2500 cluster kit V4	Illumina	GD-401-4001
Deposited data		
Raw and analyzed data	This paper	https://doi.org/10.5281/zenodo.10546916
Bulk RNAseq of cell subsets from validation cohort	Howard et al.[60]	Supplemental Table 3 from Howard et al.[60]
CITE-seq of PBMCs from individuals vaccinated with BNT162b2 mRNA vaccine	Arunachalam et al.[69]	GEO: GSE171964
Software and algorithms		
Analysis Code (and full list of R packages used)	This paper	https://github.com/niaid/fsc
scglmmr	This paper	https://github.com/MattPM/scglmmr
dsb	Mulè et al.[39]	https://github.com/niaid/dsb
R (versions 3.5.3, 4.0.5)	The R foundation	https://www.r-project.org
tidyverse (versions 1.2.1, 1.3.0)	Wickham et al.[94]	https://www.tidyverse.org
lme4 (1.1-26)	Bates et al.[95]	https://CRAN.R-project.org/package=lme4
emmeans (1.5.4)	The Comprehensive R Archive Network	https://CRAN.R-project.org/package=emmeans
limma (3.46.0)	Ritchie et al.[96]	https://bioconductor.org/packages/release/bioc/html/limma.html
fgsea version 1.24.0	Korotkevich et al.[97]	https://bioconductor.org/packages/release/bioc/html/fgsea.html
HDStIM (0.1.0)	Farmer et al.[71]	https://niaid.github.io/HDStIM/
Seurat (versions 2.3.4, 4.0.1)	Butler et al.[98]	https://CRAN.R-project.org/package=Seurat
monocle (2.10.1)	Qiu et al.[59]	https://bioconductor.org/packages/release/bioc/html/monocle.html
CellRanger	10x Genomics	https://support.10xgenomics.com/single-cell-gene-expression/software/downloads/3.1/
Multiseq	McGinnis et al.[99]	https://github.com/chris-mcginnis-ucsf/MULTI-seq
Demuxlet	Kang et al.[100]	https://github.com/statgen/demuxlet
Igraph	The Comprehensive R Archive Network	https://CRAN.R-project.org/package=igraph

RESOURCE AVAILABILITY

Lead contact

Further information and requests for resources and reagents should be directed to and will be fulfilled by the Lead Contact, John S. Tang (john.tsang@yale.edu).

Materials availability

This study did not generate new reagents.

Please cite this article in press as: Mulè et al., Integrating population and single-cell variations in vaccine responses identifies a naturally adjuvanted human immune setpoint, Immunity (2024), https://doi.org/10.1016/j.immuni.2024.04.009

CellPress

Data and code availability

- This paper analyzes existing, publicly available data. These data are included in the data repository below and accession numbers for the datasets are also listed in the key resources table.
- Code to replicate all analysis in this paper and create all figures is available in the following repository: https://github.com/NIAID/fsc. Additional preprocessing code, and the raw and processed data used in this study are available in multiple formats to facilitate reuse and reanalysis in R, python or other programming languages including standard text files, anndata, hdf5 and Seurat objects at: https://doi.org/10.5281/zenodo.10546916.
- Any additional information required to reanalyze the data reported in this paper is available from the lead contact upon request.

EXPERIMENTAL MODEL AND PARTICIPANT DETAILS

Human vaccination comparison cohorts and antibody response assessment

Healthy volunteers were enrolled on the National Institutes of Health (NIH) protocols 09-H-0239 (Clinicaltrials.gov: NCT01191853) and 12-H-0103 (www.clinicaltrials.gov: NCT01578317). The trials were approved and monitored by NIH institutional review boards in accordance with the Declaration of Helsinki and all subjects provided informed consent. Subjects enrolled in 09-H-0239 received the 2009 seasonal influenza vaccine (Novartis), and the 2009 H1N1 pandemic (Sanofi-Aventis) vaccines, both without an adjuvant. Subjects in 12-H-0103 received a vaccine formulated with the adjuvant AS03 containing avian influenza strain H5N1 A/Indonesia/05/2005 (GSK). In both cohorts, virus neutralizing antibody titers assessed using a microneutralization assay were determined as previously reported. The highest titer that suppressed virus replication was determined for each strain in the 2009 inactivated influenza vaccine: A/California/07/2009 [H1N1pdm09], H1N1 A/Brisbane/59/07, H3N2 A/Uruguay/716/07, and B/Brisbane/60/2001 or for AS03 adjuvanted influenza vaccine, H5N1 A/Indonesia, clade 2.1. High and low antibody responders to the unadjuvanted vaccination were defined using the adjusted maximum fold change (AdjMFC) which adjusts the fold change for the baseline antibody titer (methodological details in the supplementary methods of our previous report[6]). In the unadjuvanted cohort, n=10 high responders and n=10 low responders were selected for CITE-seq profiling. All subjects were analyzed pre–vaccination, with a subset of 8 and 12 donors profiled on days 1 and 7 post-vaccination also split evenly between high and low responders. In the adjuvant cohort, n=6 subjects with robust titer responses were selected for CITE-seq. Detailed subject level metadata are provided in Table S6.

METHOD DETAILS

CITE-seq profiling of peripheral blood mononuclear cells

We optimized a custom CITE-seq antibody panel of 87 markers using titration experiments and stained cells with a concentration of antibody which appeared to saturate ligand of the cell population with the highest marker expression, or used the manufacturers recommended concentration when below saturation. We stained the 52 PBMC samples across three experimental batches using aliquots of a single pool of antibodies which were combined in the optimal concentration and concentrated in an Amicon Ultra 0.5mL centrifugal filter by spinning at 14,000 x g for 5 minutes. Three aliquots of 12μL from the 36μL volume of optimized antibody mixture was used on 3 subsequent days to minimize between experiment technical variability. Frozen PBMC vials from each donor were washed in pre-warmed RPMI with 10% FBS followed by PBS. $1x10^6$ cells from each sample were stained with a hashing antibody[101] simultaneously with 1μL FC receptor blocking reagent for 10 minutes on ice. After washing the hashing reaction 3 times in cold PBS, cells were counted and pooled in equal ratios into a single tube and mixed. The sample pool was concentrated to $5x10^6$ cells in 88μL of staining buffer. 12μL of the concentrated optimized 87 antibody panel was added to stain cells (total reaction volume 100μL) for 30 mins on ice. After washing cells, we diluted cells to 1400 cells / μL, recounted 4 aliquots of cells and 30μL of the stained barcoded cell pool containing cells from all donors was partitioned across 6 lanes of the 10X Genomics Chromium Controller for each of the 3 batches for 18 total lanes. We proceeded with library prep for the 10X Genomics Chromium V2 chemistry according to the manufacturer's specifications with additional steps to recover ADT and HTO libraries during SPRI bead purification as outlined in the publicly available CITE-seq protocol (https://cite-seq.com) version 2018-02-12. We clustered Illumina HiSeq 2500 flow cells with V4 reagents with pooled RNA, ADT and HTO libraries in a 40:9:1 ratio (20μL RNA, 4.5 μL ADT, 0.5μL HTO). Libraries were sequenced using the Illumina HiSeq 2500 with v4 reagents. CITE-seq antibody information is provided in Table S5.

CITE-seq data sequence alignment and sample demultiplexing

Bcl2fastq version 2.20 (Illumina) was used to demultiplex sequencing data. Cell Ranger version 3.0.1 (10x Genomics) was used for alignment (using the Hg19 annotation file provided by 10x Genomics) and counting UMIs. The fraction of reads mapped to the genome was above 90% for all lanes and sequencing saturation was typically around 90%. ADT and HTO alignment and UMI counting was done using CITE-seq-Count version 1.4.2. We retained the "raw" output file from Cell Ranger containing all possible 10X cell barcodes for each 10X lane, and merged the CITE-seq-count output. For each 10X lane, barcodes were concatenated with a string denoting the lane of origin and data for ADT, HTO and mRNA. We then utilized combined sample demultiplexing to assign the donor ID and timepoint to each single cell. Both the timepoint and response class were identifiable based on the hashing antibody. The first round of demultiplexing was carried out via cell hashing antibodies. The union of singlets defined by the multiseq deMUTIplex procedure[99] and Seurat's HTODemux function were retained for further QC. Negative drops identified by HTODemux were retained for

Please cite this article in press as: Mulè et al., Integrating population and single-cell variations in vaccine responses identifies a naturally adjuvanted human immune setpoint, Immunity (2024), https://doi.org/10.1016/j.immuni.2024.04.009

further QC and use in denoising and normalizing protein data. The second round of sample demultiplexing was carried out via Demuxlet[100] to assign the unique donor ID by cross-referencing unique SNPs detected in mRNA single cell data against a vcf file with non-imputed illumina chip based genotype data from the same donors. Demuxlet provided an additional round of doublet removal via an orthogonal assay (mRNA) to antibody barcode (HTO) based demultiplexing thus providing further data QC. Only cells that met the following conditions were retained for further downstream QC, normalization and analysis: 1) The cell must be defined as a ''singlet'' by antibody barcode based demultiplexing and by demuxlet. 2) The identified donor from demuxlet must match one of the expected donors based on cell hashing. Cells were then further QCd based on mRNA using calculateQCmetrics function in scater.[102] Cells were removed that had with greater or less than 3.5 median absolute deviations from the median log mRNA library size.

CyTOF profiling of phospho-signaling responses after stimulation of high and low responder baseline PBMCs

Samples were thawed in a 37°C water bath and washed twice with warmed complete media with Universal Nuclease (Pierce) added. Cells were then washed a final time and resuspended in complete media. 1 million cells per condition were added to individual wells and rested in a tissue culture incubator for 2 hours (37°C, 5% CO_2). Samples were then stimulated with either PMA/Ionomycin (final concentration [10 ng/mL])/([1μg/mL]); Sigma-Aldrich), LPS (final concentration [1μg/mL]; Sigma-Aldrich), IFN-a (final concentration [10,000U/ml], PBL Assay Science), or left unstimulated. After 15 minutes at 37°C, samples were fixed with paraformaldehyde (2.2% PFA final concentration) for 10 minutes at 25°C. Samples were washed twice with Maxpar Barcode Perm Buffer (1X concentration; Standard Biotools). Samples were then barcoded with Cell-ID 20-Plex Pd Barcoding Kit (Standard Biotools) and incubated at 25°C for 30 minutes. Samples were then washed twice with Maxpar Cell Staining Buffer (Standard Biotools) and combined into corresponding barcoded batches of 5 samples (4 conditions per sample) and washed a final time with Maxpar Cell Staining Buffer. Samples were then stained with a titrated antibody-panel for extracellular markers (Table S5) for 30 minutes at 25°C. After staining, the cells were washed twice with Maxpar Cell Staining Buffer and permeabilized in methanol (Fisher Scientific) overnight at -80°C. The next day, samples were washed twice with Maxpar Cell Staining Buffer, and stained with a titrated panel of antibodies for intracellular signaling markers (Table S5) at 25°C for 30 minutes. Samples were then washed twice with Maxpar Cell Staining Buffer, and labeled with Cell-ID Intercalator Ir ([1:2000] in Maxpar Fix-Perm Buffer; Standard Biotools) overnight at 4°C. The following day, samples were washed twice with Maxpar Cell Staining Buffer and resuspended in 500μL freezing media (90% FBS (Atlanta Biologicals) + 10% DMSO (Sigma-Aldrich)), and stored at -80°C until acquisition. The day of acquisition, samples were thawed and washed twice with Maxpar Cell Staining Buffer and then once with Cell Acquisition Solution (Standard Biotools) before being resuspended in Cell Acquisition Solution supplemented with 10% EQ Four Element Calibration Beads at a concentration of 6 x 10^5 cells/mL (to approximate 300 events/sec). Samples were acquired on the Helios system (Standard Biotools) using a WB Injector (Standard Biotools). After acquisition, samples were normalized and debarcoded using the CyTOF Software's debarcoder and normalization tools (Standard Biotools). The panel and protocol were adapted for use at CHI from the Stanford HIMC.[103] CyTOF antibody information is provided in Table S5.

QUANTIFICATION AND STATISTICAL ANALYSIS

Details on the statistical testing / modeling are listed below and values reported associated with each figure are reported in the figure legend or results section text. Analysis described below was carried out with the R statistical language using base R and tidyverse collection of packages.[94]

Surface protein and mRNA count data normalization

We denoised and normalized ADT data using an open source R package we developed for this work called dsb[39] which removes noise derived from ambient unbound antibodies and cell to cell technical noise. We used the function DSBNormalizeProtein with default parameters. We normalized mRNA on the entire dataset with the normalizeSCE and multiBatchNorm functions from scran[104] using library size-based size factors. Various analysis utilized aggregated mRNA data which was were separately normalized for analysis at the subset level as a ''pseudobulk'' library; single cell mRNA data were also renormalized or rescaled for specific analysis as outlined below.

Surface protein-based clustering and cell type annotation

Using protein to define cell type facilitated improved interpretation of transcriptome differences between vaccination groups. Cell types were defined with statistically independent information, protein, from transcriptome data being modeled within each cell type (Figures 1A and 1B). We clustered cells directly on a distance matrix using the parallelDist package calculated from the non-isotype-control proteins all cells using Seurat's FindClusters function[98] using parameters: res =1.2, modularity.fxn = 1, algorithm = 3 (SLM[105]). We annotated cell types in the resulting clusters post hoc, based on canonical protein expression in immune cell populations. This procedure improved separation of known immune populations compared to compressing protein data using principal components as commonly done for higher dimensional mRNA data (data not shown). Analysis of unadjuvanted vaccination responses was first done blind to the adjuvanted cohort data. We thus first applied high dimensional clustering of the unadjuvanted cohort and annotated cell types with additional manual gates to purify canonical cell populations such as memory and naïve T cells. We next merged unadjuvanted and adjuvanted cohort cells and used annotations to guide combined clustering annotation, again manually refining cell populations using biaxial gating scripts in R to purify cell some cell populations. For annotation, the

Please cite this article in press as: Mulè et al., Integrating population and single-cell variations in vaccine responses identifies a naturally adjuvanted human immune setpoint, Immunity (2024), https://doi.org/10.1016/j.immuni.2024.04.009

distribution of marker expression within and between clusters was compared using density histogram distributions of marker expression across clusters at the single cell level, biaxial marker distribution and median and mean aggregated protein expression across clusters.

Hierarchical transcriptome variance deconstruction to infer individual (subject intrinsic), cell type, and vaccine effects

To estimate the contribution of subject intrinsic and contributors to the observed variation in expression of each gene within specific cell clusters/subsets, we used the variancePartition package.[106] The set of models used for estimating variance fractions are distinct from but related to those used for testing differential expression and contrast vaccination effects within cell subsets (see below). We first aggregated data across individual, timepoint and cell type. The normalized aggregated expression was used to first model the mean variance relationship using observation level weights using voom.[107] Mixed effects linear models of the expression of each gene across the aggregated libraries were then fitted using lme4[95] with variancePartition. For each gene "y" the total variance was defined by 780 measurements derived from the 52 PBMC samples deconvolved into the 15 major protein-based cell clusters/types tested. The model fit to each gene "g" was:

$$g = \sum_j X_j \beta_j + \sum_k Z_k a_k + \varepsilon_g$$

Where X and Z are the matrices of fixed and varying / random effects respectively, with random effects modeled with a Gaussian distribution and errors incorporating observation level weights.

$$a_k \sim N(0, \sigma_\alpha^2)$$

$$\varepsilon_g \sim N(0, diag(w_g)\sigma_\varepsilon^2)$$

The variancePartition package then incorporates both fixed and random effects in calculating the fraction of variation attributable to each variable in the model. For example, the variance in g attributable to "subjectID" (i.e., differences between individuals) was modeled as a random effect is:

$$\sigma^2_{gSubjectID} = \frac{\sigma^2_{\beta_{SubjectID}}}{\sum_j \sigma^2_{\beta_j} + \sum_k \sigma^2_{\alpha_k} + \sigma^2_e}$$

The denominator in the fraction above is the total variance of gene g, with both fixed and random effects contributing to total variance. In the first model above, age, sex, subjectID, timepoint, response /vaccine group (unadjuvanted group high vs low responders, or AS03 group) cell type, and a cell type and timepoint interaction term as categorical random effect variables as required by the variancePartition framework. As expected, a second set of models fit within each cell type/cluster (i.e., without having cell type as a variable in the model) increased the apparent variance explained by the other factors given that major cell type specific expression was a key factor driving gene expression variation. This model included age, sex, subjectID, timepoint, and response / vaccine group (as above) and an interaction term for time and group.

Within cell type linear mixed effect models of vaccination effects on gene expression

We used mixed effects linear mixed models to test coherent effects of vaccination across individuals while adjusting for subject intrinsic factors including age and sex and estimating individual subject level variation. Gene expression counts were aggregated within each surface protein-based cell type by summing counts within each sample. The lowest frequency cell types without representation across some individuals and time relative to vaccination (e.g., HSCs, donor-specific cell types, or plasmablasts which were mainly detected on day 7) were excluded from this specific analysis. Three main analyses were carried out to model gene expression within each cell type to estimate the following vaccination effects over time across individuals: model 1) unadjuvanted subjects day 1 vs baseline, model 2) unadjuvanted subjects day 7 vs baseline, model 3) A contrast of the difference in day 1 fold change between unadjuvanted and adjuvanted subjects in a combined model – the goal of this model is to assess adjuvant specific response effects. All models were fit with the 'dream' method[108] which incorporates precision weights[107] in a mixed effects linear model fit using lme4.[95] For models 1 and 2 above (unadjuvanted vaccination effects) we fit the following model: *gene ~ 0 + time + age + sex + (1|subjectID)*.

The fitted value for expression y of each gene g corresponds to:

$$y_g = \beta_{0g} + \sum_j X_j \beta_j + \varepsilon_g$$

With variables time, age, and sex represented by covariate matrix X. The β_0 term corresponds to the varying intercept for each donor represented by the (1|subjectID) term. This model thus estimates the baseline expression variation across subjects S_0 around

Please cite this article in press as: Mulè et al., Integrating population and single-cell variations in vaccine responses identifies a naturally adjuvanted human immune setpoint, Immunity (2024), https://doi.org/10.1016/j.immuni.2024.04.009

the average γ_0 using a Gaussian distribution with standard deviation ${\tau_g}^2$ to shrink estimated vaccination effects toward the population mean and adjust for non-independence of repeated measures from the same individuals, as follows:

$$\beta_{0g} = \gamma_0 + S_0$$

$$S_0 \sim N(0, {\tau_g}^2)$$

Errors ε_g incorporate observational weights w_g calculated using the function *voomWithDreamWeights* in a procedure similar to that described by Law et al.[107] but using the mixed model fit[108]:

$$\varepsilon_g \sim N(0, diag(w_g)\sigma_\varepsilon^2)$$

In this model, the day 1 or day 7 effect across subjects was the time effect from the model. The mixed model standardized z statistic was then used to rank genes for gene set enrichment testing for each cell type. Model 3 was specified as *gene ~ 0 + group + age + sex + (1|subjectID)*. The "group" variable corresponds to a combined factor representing the vaccine formulation received (adjuvanted vs unadjuvanted) and timepoint (baseline or day 1 post vaccination) with 4 level: "d0_AS03", "d1_AS03", "d0_unadjuvanted", "d1_unadjuvanted". A contrast matrix L_{delta} corresponding to the difference in fold changes between adjuvanted and unadjuvanted subjects was applied to test the null hypothesis of 0 difference in fold changes between the groups.

$$L_{delta} = [\ -\ 1\ 1\ 1\ -\ 1\ 0\ 0\ ]$$

With the first four columns representing the group factor and the two 0s representing age and sex effects. The contrast fit outputs the difference in fold change after adjusting estimates for age, sex and subject variation with positive effects representing increased fold change in the adjuvant group compared to the unadjuvanted group. This contrast approach was designed to also capture genes with opposite vaccination effects in the two groups, for example, upregulation in the AS03 group and downregulation in the nonadjuvanted subjects. Parameter estimates for each gene borrow information across genes using a mixed effects model-specific empirical Bayes procedure to estimate residual variance with a weighted mixture of chi-squares developed by Hoffman et al.[109]

Transcriptome data was uniformly processed for all fitted models above. Aggregated (summed) single cell UMI counts were normalized within each protein based cell type using the trimmed means of M values method with only genes retained with a pooled count per million above 3 using the edgeR *filterByExprs* function.[110] Cell type specific gene filtering removed genes non expressed by each lineage from analysis ensured the model assumptions used to derive precision weights and account for the mean variance trend were met. We verified the log count per million vs. fitted residual square root standard deviation had a monotonically decreasing trend within each cell type. For the AS03 validation cohort, pre normalized data were downloaded from the study supplemental data[60] and a similar model to model 3, contrasting the difference in fold change was fit with a contrast again using a donor random intercept.

Gene set enrichment testing of vaccination effects within cell types using specific hypothesis-driven gene sets or unbiased analysis

To test enrichment of pathways based on the estimated gene coefficients corresponding to the three vaccination effects defined above, we performed gene set enrichment analysis using the fgsea[97] package multilevel split Monte Carlo method (version 1.16.0). Genes for each coefficient (i.e. models 1-3) and each cell type were ranked by their effect size, (the dream package empirical Bayes moderated signed z statistic), corresponding to pre vs post vaccination or the difference in fold change for model 3 (comparing unadjuvanted vs. AS03). For enrichment of the day 1 response, five gene sets were derived from bulk transcriptomic data of influenza vaccination (Table S1), and an additional 25 pathways/gene sets curated from public databases were tested. For Day 7 responses and the difference in fold change between adjuvanted and unadjuvanted subjects, an unbiased set of pathways were tested from the Li et al. Blood Transcriptional Modules (BTM),[111] MSigDB Hallmark, reactome and kegg databases. Over-representation of GO terms for the monocyte pseudotime gene categories was assessed using enrichr.[112]

Inference of the baseline immune setpoint network

To define cell type specific transcriptional phenotypes robustly associated with high vs low responders of the unadjuvanted vaccine at baseline, we used limma[96] to fit linear models of gene expression as a function of antibody response class (high vs low, coded as a two-level factor) adjusting for age sex and batch (e.g. in R symbolic notation, gene ~ AdjMFC + age + sex + batch) as fixed effects on aggregated (summed) data for each cell type, similar to models above without varying effects for individuals:

$$y_g = \sum_j X_j \beta_j + \varepsilon_g$$

Errors incorporated voom weights as above. Gene coefficients for each cell type corresponding to model adjusted empirical Bayes regularized estimates for high vs low responder effect at baseline were input into gene set enrichment analysis against the unbiased set of pathways described above. We then calculated the average module z score[22] using log counts per million from each cell type of the high responder associated cell phenotypes (using only high responder associated leading edge genes from gene set enrichment analysis), resulting in a matrix of baseline normalized expression of pathways across 20 individuals (10 high and low responders) for

Please cite this article in press as: Mulè et al., Integrating population and single-cell variations in vaccine responses identifies a naturally adjuvanted human immune setpoint, Immunity (2024), https://doi.org/10.1016/j.immuni.2024.04.009

each cell type. We next tested for correlation of these signals, both within and between cell types, by calculating the spearman correlation and adjusted p values with the FDR method. We noticed that within the same cell type, pathway enrichments could sometimes be driven by a shared set of genes among gene sets with different pathway labels but essentially shared a substantial fraction of genes. We therefore calculated the Jaccard similarity coefficient of each pairwise enrichment signal (leading edge genes driving the high vs low responder difference) within each cell type, and use that to adjust the correlation effect sizes computed above such that the resulting quantity reflected "shared latent information" (SLI) by subtracting the Jaccard similarity index from the Spearman correlation coefficient ρ:

$$SLI = \rho - \frac{A \cap B}{A \cup B}$$

For example, given enriched pathways A and B within a cell type, if at one extreme, these two pathways are driven by the same exact shared 10 leading edge genes, the Spearman ρ of their normalized expression would be equal to 1, yet this apparent correlation is arbitrary since the two pathways reflect the same genes. However, the shared latent information would be equal to 0 because the Jaccard similarity of the two sets is also equal to 1 because leading edge genes from the two enriched pathways are the same. The remaining correlation strength better reflects the phenotypic coupling of intracellular states across individuals after removing the signal due to gene sharing between gene sets. For inter-cellular correlations between two distinct cell types, we do not subtract the Jaccard similarity of gene content from ρ as we consider the same genes to be distinct signals when measured in different cell types. We further constructed a sub network from a subset of cell types forming the high responder baseline setpoint network. To identify the most highly connected processes, correlations with adjusted p values < 0.05 were retained and a weighted undirected network was constructed using igraph, retaining only the strongest links above the median weight with weights reflecting Spearman's Rho for intercellular connections and the SLI metric described above for intracellular connections. Each node (high responder cell phenotype) was also correlated across individuals with the day 7 fold change of a gene expression signature[6] reflective of plasmablast activity derived from bulk microarray data from the same subjects and select high degree nodes were highlighted in the text.

Single-cell mixed-effect models of gene expression

In addition to the pseudo-bulk models fitted above, we also used single cell mixed effects models to assess consistency and to specifically test the early response kinetics of the baseline states enriched above, including select AS03 associated response signatures within innate immune cell subsets.

Early kinetics of baseline setpoint phenotypes

Each cell type specific transcriptional phenotype enriched in high vs low responders in the aggregated/pseudo-bulk linear model described above were scored in single cells from subjects on day 0 and day 1 as the average expression of the specific leading edge genes enriched in high vs low responders. The per single cell module scores were fitted with a linear mixed model for each cell type to 1) re-test the baseline association (high vs. low responders) at the single cell level, and 2) to test their post vaccination effect size within the same cell subset. These models estimated the variance at the single-cell level instead of at the individual donor cell-aggregated level. Otherwise these represent conceptually similar models as the ones described above fitted using lme4 with a donor random intercept, but without voom weights. Two models were tested with highly concordant resulting effect sizes: 1) a parsimonious model of time relative to vaccination with a subject random effect, and 2) a more complex model including the time relative to vaccination, the number of cells per individual sample for a given cell type, age, sex, and a subject random effect. Normalized expression of each module was standardized within each surface protein-based cell cluster/subset by subtracting the mean and dividing by the standard deviation of the module score across single cells within the cell type. After fitting models, the baseline high vs low responder effect and the day 1 vs baseline effect sizes and standard errors across subsets was calculated using the emmeans[113] package with a custom contrast (e.g., see Figure 4E). All models were checked for convergence criteria.

AS03 specific regulation

Naïve B cells were tested for expression of modules hypothesized to be involved in B cell survival (see below; partly based on the literature or derived from existing independent data sets). These modules were tested here for their effects at the single cell level; they were then independently assessed in sorted total B cells in the validation cohort.[60] Two modules were defined to reflect survival of human naïve B cells: 1) A CD40 activation signature[22] which was derived from studies of in vitro CD40 activated human B cells; 2) An apoptosis signature derived by combining signals from the CITE-seq naïve B cell day 1 gene set enrichment comparing AS03 adjuvanted to unadjuvanted individuals. The signals combined the specific naïve B cell leading edge genes from the negatively enriched (reflecting AS03 specific downregulation) apoptosis modules (with unadjusted p values < 0.1–we opted for a loser cutoff to increase sensitivity): reactome activation of BH3 only proteins, Reactome intrinsic pathway for apoptosis, and LI.M160 leukocyte differentiation. The cell type specific leading edge genes were scored as above and fitted with age and sex covariates, a combined factor for vaccine group, timepoint, and random effect for subject ID, with the difference in fold changes calculated using the emmeans package.

Software for implementing analysis workflow

The analysis framework described above is available in an R software package "scglmmr" (https://github.com/MattPM/scglmmr) for analysis of single cell perturbation experiment data with repeated measures and multi-individual nested group designs. The software provides workflows for fitting single cell mixed models, deriving cell signatures, visualization, wrapper functions to implement the

Please cite this article in press as: Mulè et al., Integrating population and single-cell variations in vaccine responses identifies a naturally adjuvanted human immune setpoint, Immunity (2024), https://doi.org/10.1016/j.immuni.2024.04.009

weighted gene level mixed effects differential expression models described Hoffman and Roussos[108] (dream), enrichment using fgsea, and the network analysis methods described above.

Monocyte differentiation and perturbation pseudotime analysis

To construct a combined monocyte differentiation and perturbation single cell map we used the DDR tree algorithm (Discriminative Dimensionality Reduction via learning a tree) with monocle 2.[59] The trajectory was constructed using the genes that changed as a function of time (q value <0.15 using the differentialGeneTest in monocle, with ribosomal genes and genes expressed in less than 15 cells removed). The DDRtree algorithm[58] was implemented using the monocle function reduceDimension with arguments *residualModelFormulaStr* = subjectID and max_components = 2 and pseudotime calculated with function orderCells. Independently of the genes used to construct the trajectory, we then tested the genes from the mixed effects model of vaccination effects from monocytes (specific leading edge genes from 'reactome interferon signaling', 'GO IL6 PRODUCTION', 'reactome IL4 and IL13 signaling', 'HALLMARK inflammatory response', 'KEGG JAK STAT signaling') for branch dependent differential expression using the *BEAM* function from monocle. Select genes were highlighted and categorized based on their expression dynamics along real time and pseudotime.

Cell frequency analysis

Cell frequencies of activated monocytes gated as HLA-DR$^+$ cells were computed as a fraction of total CD45+CD14+ classical monocytes using flow cytometry data.[6] These cell frequencies were compared across subjects (high vs. low responders) at baseline using a two sided Wilcoxon rank test. The kinetic change of the cell frequency following vaccination was modeled using a mixed effects model with a single random effect for subject ID similar to the models described above. The kinetics over time were modeled using an interaction for time and antibody response group (high vs. low AdjMFC). This interaction model was compared to a timepoint only without the group interaction effect with analysis of variance. The baseline versus day 1 effects for each antibody response group was calculated using the emmeans package.

Analysis of phospho-signaling responses after stimulation of high and low responder baseline PBMCs using CyTOF

The protein phosphorylation markers driving the stimulated phenotype and responding cells were automatically defined using the HDStIM R package.[72] The median anti-phosphorylated protein heavy metal-labelled antibody intensity for each individual sample and cell type and stimulation was calculated and modeled with a mixed effects model adjusting or batch and using a random effect for donor ID. The difference in fold change between unstimulated and stimulated cells was calculated using a custom contrast with the emmeans package.